Kinetic stability of metal–organic frameworks for corrosive and coordinating gas capture

Kinetic Stability of Metal-Organic Frameworks: Consequences for Corrosive and Coordinating Gas Capture

Adam J. Rieth[1], Ashley M. Wright[1], and Mircea Dincă[1]*

[1] Department of Chemistry, Massachusetts Institute of Technology, 77 Massachusetts Ave. Cambridge, Massachusetts, 02139, United States.

* Correspondence to: mdinca@mit.edu

Abstract

Metal-organic frameworks (MOFs) have demonstrated their utility for a variety of applications involving the storage, separation, and sensing of weakly interacting gases of high purity. Exposure to more realistic, impure gas streams and interactions with corrosive and coordinating gases raises the question of chemical robustness, which remains a paramount concern for practical applications of MOFs. However, factors that determine the stability of MOFs remain incompletely understood. Although past researchers attempted to categorize framework materials as either thermodynamically stable or kinetically stable, recent work has elucidated an energetic penalty for porosity for all materials in this class with respect to a dense material. The metastability of porous phases has important implications for the design of materials for gas storage, heterogeneous catalysts, and electronic materials. Here, we focus on two main strategies for stabilization of the porous phase, either by using inert metal ions, or by increasing the heterolytic metal-ligand bond strength, both of which increase the activation barrier for framework collapse. These two strategies have led to exceptionally robust materials for the capture of coordinating and corrosive gases such as water vapor, ammonia, H_2S, SO_2, NO_x, and even elemental halogens, and we review the progress in designing stable materials for these gases. Looking forward, we envision that the continued pursuit of strategies for kinetic stabilization in the synthesis of new MOFs will provide increasing numbers of robust frameworks suited to harsh conditions, and that short-term stability towards these challenging gases will be predictive of long-term stability for applications in less demanding environments.

Introduction

Porosity is a useful and versatile material property for a range of current and future applications, including gas storage,[1–4] chemical separations,[5–7] catalysis,[8–10] and electronic devices.[11,12] Yet, much like a cavern's susceptibility toward cave-in, the empty voids of porous materials also imply the possibility of collapse. Therefore, in order to be applicable, the stability of porous materials is of eminent importance. Metal-organic frameworks (MOFs) are materials consisting of regular arrays of metal ions or clusters linked by organic ligands, and they can exhibit record internal surface areas.[13] Research into MOFs, and concomitantly the number of possible applications for these materials, has increased exponentially over the past several years. However, they are not yet widely applied in industry, and in many cases the deployment of MOFs is held back by a lack of long-term stability under environmental or application-specific conditions. Here, we focus on framework chemical stability toward coordinating and corrosive gases and vapors, such as water vapor, NH_3, H_2S, Cl_2, Br_2, NO_x and SO_x, which may be present in the atmosphere, or as components in applications for which MOFs find utility.

The Energetic Penalty for Porosity

Horror Vacui, a phrase attributed to Aristotle roughly translated as *nature abhors a vacuum*, was, until recently, thought to apply to the crystallization of permanently porous solids. Porous solids were believed to be unstable due to the relative lack of bonding or dispersive interactions within or between the voids.[14] Of course, materials such as zeolites and MOFs are now commonly synthesized, normally by including solvent, surfactant, or structure-directing agents within the voids during crystallization, although the degree of kinetic or thermodynamic control responsible for their formation is still under debate.[15] After the porous material is synthesized, the components within the pores are commonly removed by evacuation or annealing, leaving behind accessible voids. However, an increasing body of work suggests that crystalline porous materials with empty pores are metastable with respect to their dense phases (**Figure 1**).[16–21] The dense phase is a hypothetical assemblage of the same constituent atoms, ions, or ligands, but carries negligible porosity. For an all-silica zeolite, the dense phase is easily envisaged as nonporous amorphous silica, which can be accessed via simple heating. For a MOF, the dense phase can be more difficult to conceptualize due to the directionality of the ligands, but denser, amorphous phases of some MOFs, achieved thermally, are known,[22–25] and other structures transition to denser amorphous phases with the application of pressure.[26–28]

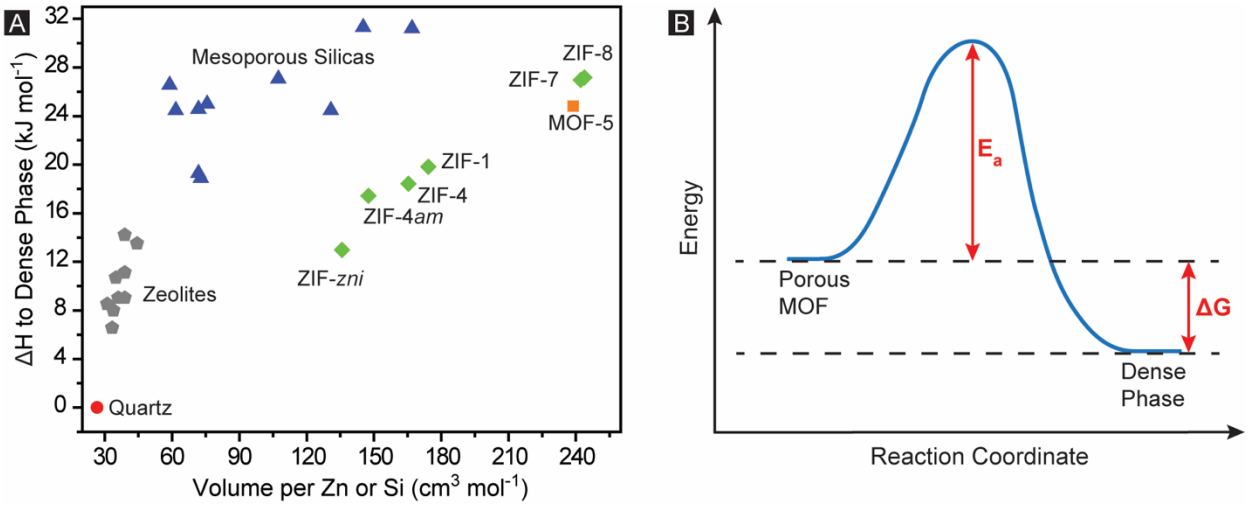

Figure 1: **Metastability of Porous Materials.** A) Enthalpic penalty relative to a dense phase versus molar unit cell volume per Zn or Si for porous materials including zeolites, mesoporous silicas, ZIFs, and MOF-5.[16,17,20] B) Conceptualization of the energy penalty for porosity in a reaction coordinate diagram.

The metastability of solvent-free porous materials has been experimentally demonstrated for many zeolites,[19] zeolitic imidazolate frameworks (ZIFs),[17] as well as the prototypical MOFs $Zn_4O(BDC)_3$ (MOF-5, BDC = 1,4-benzenedicarboxylate)[16] and $Cu_3(BTC)_2$ (HKUST-1, BTC = 1,3,5-benzenetricarboxylate).[18] Inclusion of solvent in the thermodynamic equations can result in a thermodynamically stable porous phase (with respect to the dense phase) in the case of HKUST-1,[18] whereas inclusion of solvent for MOF-5, though highly exothermic,[21] is insufficient to result in net stabilization.[16] Regardless of the thermodynamics of the solvent-inclusive phase, for the majority of applications the evacuated phase is desired. It has been argued that the increased vibrational entropy of porous phases of MOFs could represent enough energetic

stabilization to account for a net negative free energy with respect to dense phases at slightly elevated temperatures.[15] However, the available calorimetric data indicate a trend of increasing energy penalty for increasingly porous structures, and a dense, amorphous phase should be entropically favored over a crystalline porous phase given that the driving force for crystallization is commonly enthalpic.[20]

Kinetically Stabilizing the Porous MOF Phase

Conceptualizing MOFs with empty pores as metastable, kinetically-trapped phases has important implications for the development of design principles for chemically stable frameworks. Stabilization of the porous phase can only be kinetic and must increase the energy barrier for transitioning to the dense phase by 1) increasing the transition state energy or 2) decreasing the energy of the porous phase with respect to the transition state (**Figure 2**).

1) Metal Ion Substitution Kinetics: increasing the transition state energy

Transitioning from a porous MOF phase to a dense phase must require ligand exchange or geometric reorganization around the metal ion. A major component in the energy barrier for reorganization towards a dense phase is contained in the inherent kinetics of ligand exchange of the metal ion. As a consequence of electronic configuration and of ionic radius, transition metal ions can exhibit vastly disparate ligand exchange kinetics, which are most often quantified by the homoleptic aquo complex self-exchange rate. The rate of ligand exchange in octahedral aquo complexes spans nearly twenty orders of magnitude from the labile Cu^{2+} and Cr^{2+} at 5.9×10^{9} s^{-1} to the highly inert Ir^{3+} at 1.1×10^{-10} s^{-1}.[29] MOFs formed with kinetically inert metals can be exceptionally robust. For instance, the most widely employed metal ion in MOF synthesis with a metal-aquo self-exchange rate slower than 1 s^{-1} is Cr^{3+}, which forms carboxylate frameworks stable to water, steam, and even high pressures of H_2S.[30–32] Cation inertness can be a better predictor of stability than metal-ligand bond strength, as was demonstrated in the MIL-53 and -47 family of isostructural frameworks where chemical stability decreases in the order $Cr^{3+} > Al^{3+} > V^{4+}$, as expected based on the water substitution rates of the metal-aquo complexes, but not in line with the thermodynamic metal-oxygen bond strength.[33] An additional example of the effects of inert metal ion substitution can be found in the M_2DOBDC (MOF-74 or CPO-27, DOBDC = dioxidobenzenedicarboxylate)[34,35] family of frameworks, where partial replacement of Mg^{2+} with more inert Ni^{2+} can enhance the stability toward water.[36] Replacement of the native Zn^{2+} with Ni^{2+} in MOF-5 also grants increased water stability for the resulting Ni-MOF-5.[37] Further, in a family of MOFs formed from linear bistriazolate linkers, M_2Cl_2BBTA (BBTA = bibenzotriazolate)[38,39] and M_2Cl_2BTDD (BTDD = bistriazolodibenzodioxin),[40,41] stability towards water and ammonia decreases in the order $Ni^{2+} > Co^{2+} > Mn^{2+} > Cu^{2+}$, in agreement with the trend in metal-aquo substitution rates.[42,43] Based on these examples, the metal ion ligand substitution rate is a systematic descriptor of MOF stability that nevertheless is less recognized in the literature.

The trend in stability for MOFs based on ligand exchange rate is distinct from the stability trends for divalent metal complexes observed by Irving and Williams,[44,45] with the most notable divergence being many Cu^{2+} materials. Due to the d^9 electronic configuration of Cu^{2+}, resulting in a Jahn-Teller distortion, its complexes exhibit relatively short, strong bonds to four equatorial ligands, accounting for the high measured stability constants for ligand complexes, but also exhibit extremely rapid ligand exchange at axial positions, resulting in lower observed stability for many Cu^{2+} MOFs than what would be expected from the Irving-Williams series.

2) Bond Strength: stabilizing the porous phase relative to the transition state

The weakest link in a MOF is commonly the metal-ligand bond. Substantial previous literature has demonstrated that stability towards polar analytes can be augmented by increasing the heterolytic metal-ligand bond strength,[46–49] a result of lowering the energy of the porous framework relative to the heterolytic bond-breaking transition state.[50] For example, MOFs formed using pyrazolate or imidazolate ligands in combination with late transition metals often exhibit superlative chemical stability, which can be attributed to the stronger donating ability of these ligands versus carboxylates, and can be quantified by the ligand basicity. Metal-binding groups that are more donating will increase the heterolytic metal-ligand bond strength, particularly for late transition metals, and enhance MOF stability, up to a point. Ligands with greater donating ability than pyrazolates have not been widely explored in MOF chemistry, due largely to synthetic difficulties in either accessing the ligand or crystallizing the framework. Yet increasing the donating ability significantly more may not result in increased stability towards water because of the concomitant increase in driving force for metal-ligand bond hydrolysis.

An additional strategy for increasing the metal-ligand bond strength for carboxylate frameworks is to increase the valency of the metal ion. Although augmenting the ligand donation strength is successful for late transition metals because it results in a stronger, more covalent bonds, increasing the ionic bond strength is also possible when employing carboxylate ligands by simply increasing the charge density on the metal ion. Higher-valent metals paired with carboxylates, such as Ti^{4+}, Zr^{4+}, Cr^{3+}, and Al^{3+} will form stronger metal-ligand bonds than those constructed with divalent metal ions.

Although increasing the metal-ligand bond strength is often thought of as a route towards the thermodynamic stabilization of the porous phase, there may be no net change in the driving force towards the dense phase because the dense phase with the same metal-ligand bond is equally stabilized. For instance, moving from carboxylate (pK_a(DMSO) = 11.1)[51] to imidazolate (pK_a(DMSO) = 18.6)[52] in Zn^{2+} frameworks results in nearly identical energy penalties for the porous MOFs, MOF-5 and Zn-methylimidazolate (ZIF-8), with respect to the corresponding dense phases.[17] Nonetheless, the increased metal-ligand bond strength of ZIF-8 does result in greater kinetic stability relative to MOF-5, especially towards coordinating species, due to an increased energy barrier for heterolytic metal-ligand bond breaking.[50]

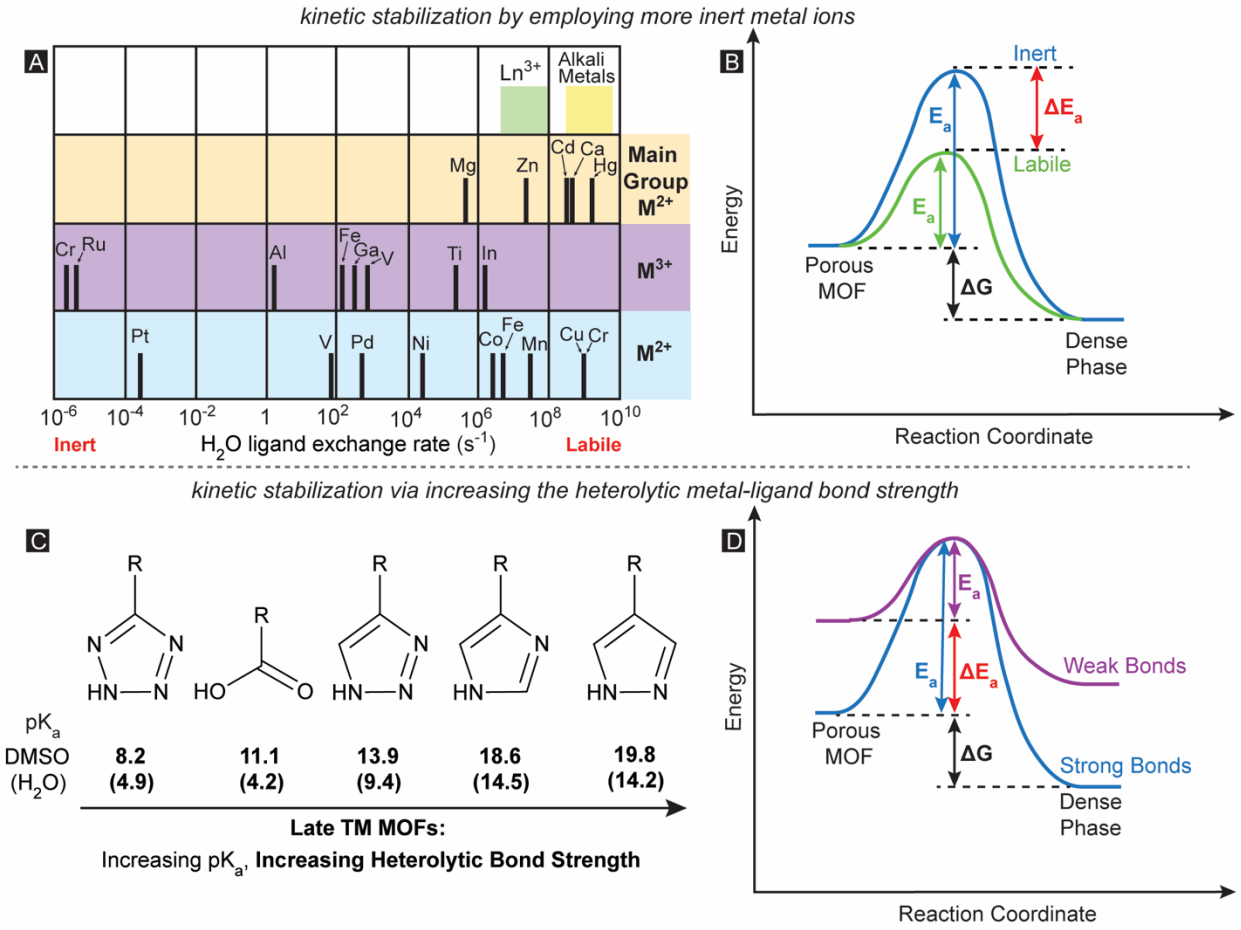

Figure 2: **Routes towards kinetic stabilization of MOFs.** Methods towards stabilization of the porous phase with respect to the dense phase must involve increasing the activation energy barrier. A) Metal-aquo self-exchange rate constant for various metal ions.[29,53,54] B) Metal ion inertness increases the activation energy barrier for rearrangement to the dense phase. C) The use of more strongly donating azolate ligands, as measured by pK_a,[51,52,55] in combination with late transition metals, results in stronger metal-ligand bonds. D) Increasing the heterolytic metal-ligand bond strength results in a greater activation energy barrier for a bond-breaking transition state, while not affecting the net driving force towards the dense phase.

Linker and node connectivity

The transition state energy can additionally be boosted by increasing the connectivity of framework components, improving stability in a manner similar to the chelate effect. The stabilization comes as a result of increasing the number of metal-ligand bonds which must dissociate or rearrange simultaneously in order for a phase transition to occur or a pore to collapse. For instance, the barrier to linker removal or reorganization will be greater for a tetratopic carboxylate, such as the linker of NU-1000 ($Zr_6O_4(OH)_4(HCOO)_4(TBAPy)_2$, TBAPy = pyrene tetra-*p*-benzoic acid),[56] than a ditopic carboxylate, such as the biphenyl dicarboxylate (BPDC) linker of UiO-67 ($Zr_6O_4(OH)_4(BPDC)_6$).[57] Similarly, frameworks made up of secondary building units (SBUs) with greater connectivity exhibit enhanced stability, exemplified by MOFs constructed from Zr^{4+} oxo-hydroxo nodes which may be linked by 6, 8, 10, or 12 carboxylate groups, whose stability generally covaries with node connectivity.[58–60]

Sterics and Hydrophobicity:

Steric shielding of metal-ligand bonds can impede the access of water and other coordinating vapors to delicate metal-ligand linkages.[60–64] However, this strategy also may decrease overall porosity as well as inhibit the access of desirable sorbates to the framework sites, which often exhibit the strongest guest binding interactions.

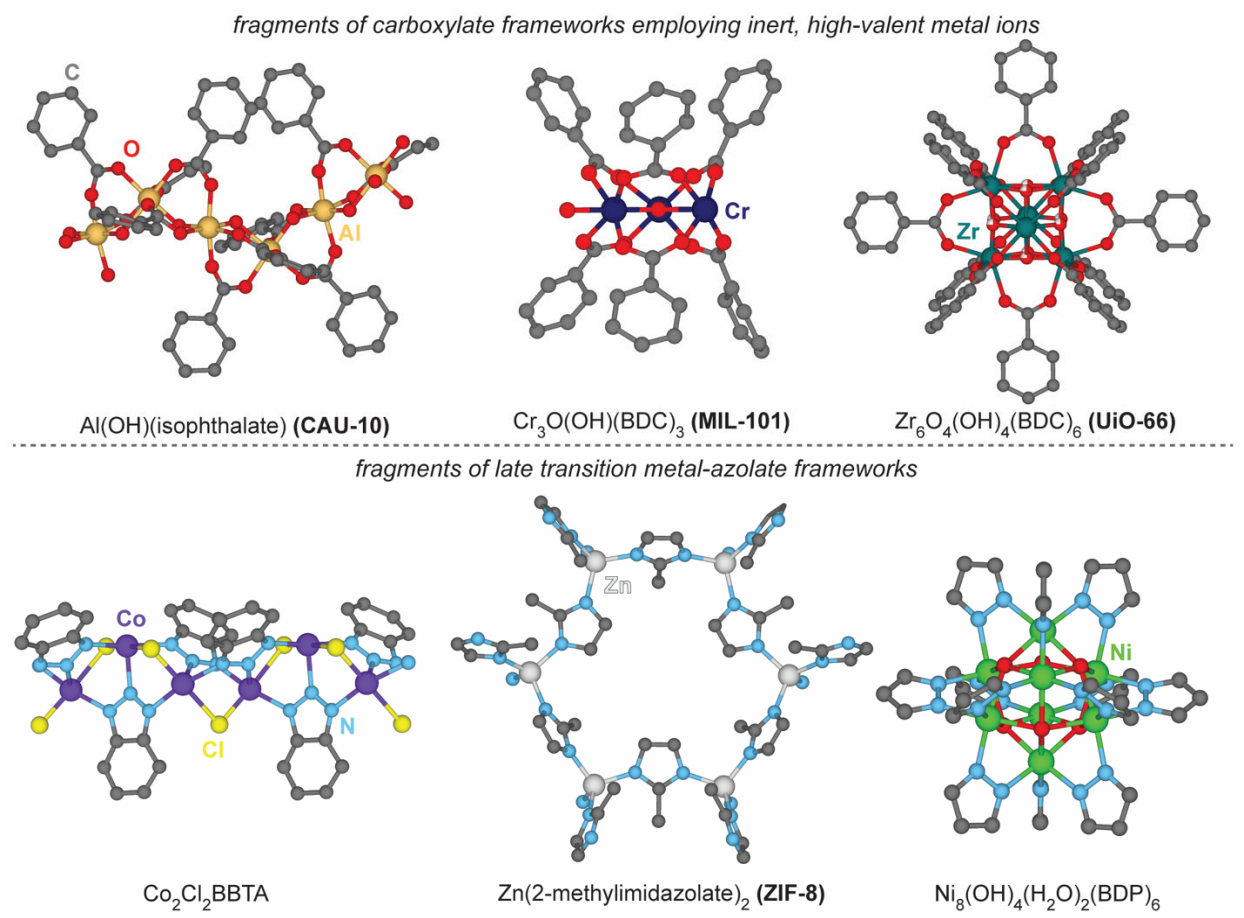

Figure 3: **MOF building blocks with high kinetic stability.**[30,38,57,65–67] BDP = 1,4-benzene-dipyrazolate. H atoms omitted for clarity.

Effects of Gases and Vapors on Framework Stability

Coordinating Gases and Vapors: H_2O, NH_3, H_2S

Perturbations in the bonding and connectivity of a MOF frequently result in decreases in the useful surface area and porosity. Framework exposure to coordinating gases and vapors are one cause of such perturbations. The ability of a MOF to withstand exposure is directly related to the energy barrier towards ligand rearrangement or substitution. Several reaction pathways can be operative, including ligand substitution,[50] metal-ligand bond hydrolysis,[68–70] coordination-induced ligand rearrangement,[71,72] or pore collapse due to capillary forces.[73,74] Common to all mechanisms is a requirement for ligand rearrangement around the SBU, as well as some degree of heterolytic metal-ligand bond breaking. These factors directly relate the stability of a MOF towards coordinating gases and vapors to the kinetics of ligand exchange at the metal center, as well as the heterolytic metal-ligand bond strength. For example, theoretical calculations for

metal-ligand hydrolysis and water substitution reactions reveal that hydrolysis to form the metal hydroxide and the protonated ligand is universally downhill for diverse frameworks including Zn-MOF-5, Cu-HKUST-1, Cr-MIL-101, and Zn-ZIF-8, but the activation energy barrier for ligand substitution is much larger for Cr-MIL-101 and Zn-ZIF-8, in line with the experimentally observed high steam stability for these two frameworks versus Zn-MOF-5 and Cu-HKUST-1.[50]

The stability trends of MOFs towards polar gases is largely dependent on the gas' acidity as well as its nucleophilicity. The stability of MOFs towards NH_3 and H_2S trend with the stability for water. However, the greater nucleophilicity of NH_3 makes ligand substitution potentially more favorable. In combination with water, ammonia forms NH_4OH, which is highly corrosive and may result in metal ligand bond hydrolysis.[75] Moving to the more acidic H_2S, with a pK_a of 7.0 in water, seven orders of magnitude more acidic than H_2O, protonation of the ligand occurs more readily, resulting in a metal sulfhydryl or sulfide.[32] Further, H_2S is strongly nucleophilic and coordinating to metal ions, therefore it can readily substitute for a framework ligand.

Acidic and Oxidizing Gases and Vapors: SO_x, NO_x, elemental halogen X_2

Designing materials that are stable to acidic and oxidizing gases such as sulfur dioxide (SO_2), nitrogen oxides (NO_x), and halogens (X_2) present unique challenges. In particular, oxidation of the metal center by an oxidizing gas can drastically alter the kinetics of ligand substitution as well as the preferred ligand geometry around a metal center. Further, many materials are stable to corrosive gases in single component studies, but in the presence of humid air a variety of new challenges arise from potential side reactions that form strong acids.[76] For instance, in combination with water vapor, SO_2 forms sulfurous acid (H_2SO_3), and over time in the presence of oxygen it can form SO_3 and sulfuric acid (H_2SO_4).[77] Consequently, SO_2 adsorption in humid air, most relevant for industrial applications, is challenging, and linker protonation resulting in the formation of metal sulfites or sulfates can be extremely destructive.[78]

The capture of NO_x presents additional challenges. Much the same as SO_2, both NO and NO_2 under humid conditions can form the strong acids HNO_2 and HNO_3, which may protonate linkers to cause framework degradation. NO and NO_2 can also undergo a variety of redox reactions, such as NO disproportionation ($3\ NO \rightarrow NO_2 + N_2O$), NO oxidation ($2\ NO + O_2 \rightarrow 2\ NO_2$), or NO_2 dimerization/disproportionation ($2\ NO_2 \rightarrow N_2O_4 \rightarrow NO^+ + NO_3^-$).[79]

Formation of NO^+ can be very destructive as it may react with aromatics, amino groups, or transition metals to cause irreversible framework damage. Therefore, in order to design frameworks for NO_x capture, it is important to either employ methods to mitigate the reactive chemistry of NO_x or to design materials that accommodate the daughter products.[80]

Framework Design for Strongly Interacting Gas Capture

The modularity of MOFs allows for three main strategies towards increasing the interaction strength between the framework and polar gases. The first approach relies on MOFs containing metal ions with open coordination sites, typified by frameworks such as HKUST-1, MOF-74, and M_2Cl_2BBTA. These frameworks can exhibit strong affinities for Lewis basic gases as well as oxidizing gases. However, direct coordination by an analyte gas to a framework node can lead to ligand rearrangement or hydrolysis of the metal-ligand bond. Therefore, the deployment of this method requires robust stability. The second strategy focuses on the installation of functional groups, such as $-NH_2$, -OH, or $-SO_3H$ moieties, on the organic ligands. This approach can effectively modulate framework polarity and hydrophilicity. However, the

functional groups occupy pore volume and reduce the surface area of the resulting frameworks. Thirdly, auxiliary ligands integral to the SBU can be leveraged as strongly interacting sites for polar gases. For instance, the μ-OH moieties in $Zr_6O_4(OH)_4^{12+}$ SBUs can serve as primary sorption sites for water as well as SO_2.[58,81] It should be noted that augmenting the surface area, although it may increase the overall capacity for gas uptake at high relative pressure, does not result in improved affinity for polar gases at low relative pressure. While the number of purely dispersive interaction sites increases with higher surface area, these weak binding sites are insufficient for selective polar gas capture.

H_2O

Occurrence, Applications:

The stability of MOFs towards water has been extensively investigated[58–60,82] because it is the most common coordinating and corrosive gas present in the atmosphere as well as in many applications like postcombustion gas streams,[6,83] gas sensing,[84] or in fuel cells requiring proton conducting materials.[85] Additionally, the capture of water vapor has several desirable applications including dehumidification,[73,86,87] heat transfer,[88,89] and atmospheric water capture.[41,90–94] These applications all rely on cycles in which water alternatively fills the pores, and then is desorbed, creating a requirement for extensive cycling stability. Water is unique among the gases and vapors considered herein because it is a liquid at STP and will thus completely fill the entire pore interior of a porous material above a suitable humidity. Strategies for the design of water sorbents have focused on optimizing the relative humidity (RH) of pore filling, such that it is favorable under the temperature and vapor pressure conditions of a given application. The partial pressure of pore filling is highly dependent on the pore size as well as the pore hydrophilicity. Smaller pores fill at lower RH and larger pores fill closer to 100% RH.[58,82,95] Additionally, framework hydrophilicity may be modulated by appending polar groups to the organic ligands. As above, this strategy results in a reduction of total pore volume and it leads to broadening of the water uptake step, both of which equate to a lower usable capacity.[48,96–98] Anion and cation exchange strategies at the node can control the partial pressure of pore filling without modifying pore size and shape, but may require careful consideration of the changes to framework stability inherent to SBU alterations.[99]

MOF Sorbents for H_2O:

Water sorbents with extended cycling stability generally fall into two categories: 1) High-valent inert early transition metal-carboxylate frameworks, and 2) Late transition metal-azolate frameworks. The stability of MOFs towards water has been reviewed several times previously,[60,82] and a comprehensive review of all MOFs investigated for water sorption is available.[89] Here we focus on the trends in stability for MOF building blocks and the superlative sorbents constructed from the more stable building blocks.

1) Inert, high-valent metal carboxylates

Zr^{4+} MOFs featuring $Zr_6O_4(OH)_4(RCOO)_{12}$ nodes, typified by the terephthalate-linked UiO-66[57] have been widely explored as stable water sorbents.[100] Varying the ditopic carboxylate linker from the smallest (fumarate, MOF-801)[101] to the largest (4,4′-[(2,5-Dimethoxy-1,4-phenylene)bis(ethyne-2,1- diyl)]dibenzoic acid, PIZOF-2)[102] results in the controlled modification of the pore size from 6 Å to 20 Å, enabling the tuning of the water uptake step from 9% RH to 75% RH.[58] Although Zr^{4+} carboxylate frameworks are generally thought of as stable to water, this is not the case for all members of the family. MOF-805, -806 and -808 were found

to degrade significantly with water sorption, whereas MOF-801, MOF-802, MOF-841, and UiO-66 were found to be stable to at least five cycles of water uptake and release.[58] Differences in the stability of hexanuclear zirconium frameworks are often attributed to the connectivity of the node, as well as the rich defect chemistry of zirconium MOFs,[74,103–106] with more defective frameworks collapsing faster due to their lower connectivity. Recently, MIP-200 ($Zr_6O_4(OH)_4(HCOO)_4$(methylene diisophthalate)$_2$) was reported to have a water capacity of nearly 40 percent by weight (wt%) achieved below 25% RH and further, the framework exhibits exceptional chemical and water cycling stability over 50 cycles, attributed to residual extra-framework anions bound to the nodes. MIP-200 withstands NH_4OH vapor, 6M H_3PO_4, aqua regia, HNO_3, and HCl at reflux.[107]

Nodes consisting of inert Al^{3+} ions linked by carboxylates, commonly forming oxo-centered trinuclear SBUs found in $Al_3O(OH)(BTC)_2$ (Al-MIL-100),[108,109] or infinite chains of Al^{3+} bridged by hydroxo groups, an SBU found in Al(OH)(BDC) (Al-MIL-53),[110] make up another family of exceptionally stable carboxylate MOFs. One of the most mass-produced MOFs, Al(OH)(fumarate), isoreticular to MIL-53, has been tested on a full-scale heat exchanger for heat transfer processes. This MOF coating exhibited a 95% capacity retention for water after 360 cycles.[111] Aluminum MOFs formed with bent dicarboxylate linkers, typified by CAU-10 (Al(OH)(isophthalate))[65,112,113] exhibit exceptional water sorption characteristics for heat transfer processes. CAU-10 is extremely scalable[114] and has a water isotherm step well positioned to be of use in adsorptive heat transfer processes. Extensive water cycling of a heat exchanger coated with a sample of CAU-10 in a binder resulted in a negligible loss in capacity after 10,000 cycles.[112] Moving to the lighter-weight 2,5-furandicarboxylate linker produces the isostructural MIL-160 framework,[115] which has an increased water affinity as well as augmented gravimetric water capacity. Further, the recently reported Al-MOF-303 employs 2,5-pyrazole dicarboxylate as the linker, and retains its water capacity of 33 wt% after 150 cycles.[94]

The most kinetically inert of the first-row transition metals, Cr^{3+} forms exceptionally robust frameworks with multitopic carboxylates. Cr^{3+} frequently forms SBUs similar to those formed by Al^{3+}. For instance, $Cr_3O(OH)(BTC)_2$ (Cr-MIL-100) and Cr-MIL-101[30] are made up of trinuclear oxo-centered clusters, and Cr(OH)(BDC) (Cr-MIL-53)[31] consists of infinite chains of metal ions bridged by hydroxo groups. Cr-MIL-101 has been widely explored for water sorption due to its exceptional overall water uptake of 1.6 g g^{-1} as well as its superlative cycling stability.[97,116–118] As a consequence of its exceptional inertness, the synthesis of Cr^{3+} frameworks present substantial challenges due to the irreversibility of bond-forming on a reasonable timescale. In order to obtain water sorbents with both high capacity and exceptional stability, one strategy to overcome the difficulties of direct Cr^{3+} MOF synthesis is to first crystallize an Fe^{3+} carboxylate framework, and subsequently use cation exchange of Cr^{2+} for Fe^{3+} in order to incorporate chromium into the framework. The labile Cr^{2+} is able to rapidly enter the SBU, and once inserted, it is oxidized by Fe^{3+} to Cr^{3+}, which is thereby kinetically trapped. This strategy was pursued to synthesize the record-setting Cr-*soc*-MOF,[73,119] which can uptake nearly 2 g g^{-1} water, as well as the Cr-*acs*-MOF termed NU-1500.[120] Testament to the fundamental analysis presented earlier, the Fe^{3+} analogs, as well as the Al^{3+} analog for the mesoporous *soc*-MOF, collapse due to capillary forces during pore filling or when activated from water, whereas the Cr^{3+}-exchanged frameworks withstand repeated water cycling.[73,120]

Carboxylate frameworks incorporating other metal ions including Ti^{4+} and Fe^{3+} have also been investigated for water sorption applications. $Ti_8O_8(OH)_4^{12+}$ nodes are among the more stable building blocks for MOFs. $Ti_8O_8(OH)_4(H_2N\text{-}BDC)_6$ (Ti-MIL-125-NH_2) absorbs more than

50 wt% water below 25% RH, with minimal loss of capacity over 10 cycles.[121] Additionally, $Fe_3O(OH)(BTC)_2$ (Fe-MIL-100) was investigated for latent cooling load reduction dehumidifying climate control air streams, and a MOF coating on a heat exchanger could be cycled 2000 times, while losing only 4.5% of the original capacity.[86] Carboxylate MOFs employing transition metals later or lower-valent than Fe^{3+} are not candidates for water sorption applications due to stability concerns.

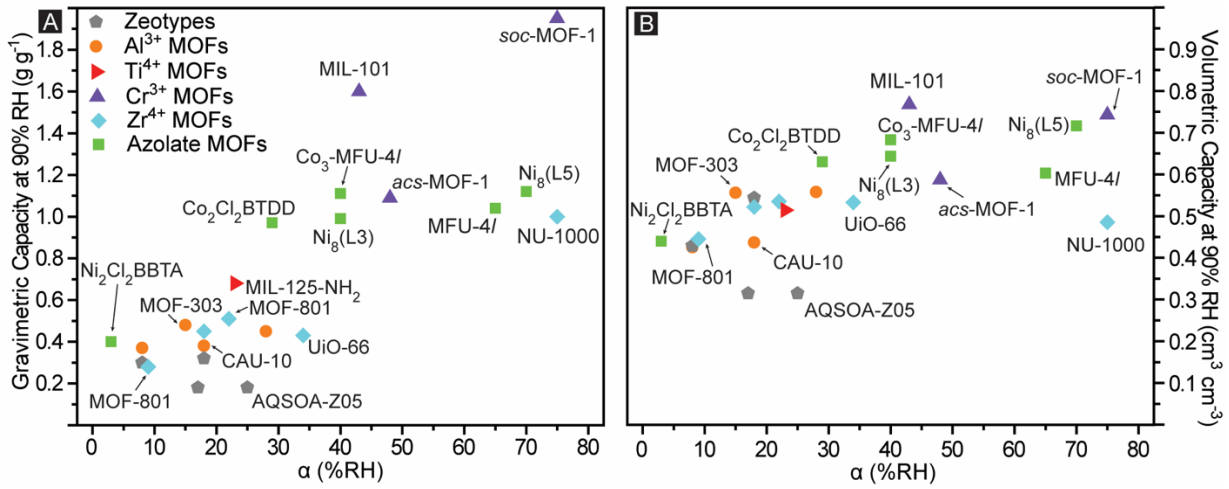

Figure 4: **Water Capacities of Porous Solids.** A) Gravimetric uptake capacity versus α, the RH value at which half the total capacity is reached. Materials with larger pores can achieve higher gravimetric capacities with concomitant reduction in hydrophilicity. B) Plotting the capacity in volumetric units highlights the significantly reduced variation in total capacity as a function of hydrophilicity. Values and references listed in **Table 1**.

2) Late transition metal azolate frameworks

Moving from the hard, weakly donating carboxylate ligands to the comparatively soft, strongly donating azolate ligands such as triazolate, pyrazolate and imidazolate engenders heterolytically stronger metal-ligand bonds with late transition metals. This strategy has been effective in creating robust Zn^{2+} MOFs with imidazolates and pyrazolates, even though Zn^{2+} is quite labile. The ZIFs have been widely explored as water sorbents and exhibit exceptional stability, yet their general hydrophobicity as well as their limited total pore volume, which governs the total deliverable capacity, restricts the utility of ZIFs in applications such as heat transfer and water harvesting.[89,116] Pyrazolate frameworks have been explored as water sorbents for heat transfer, however, the topologies heretofore synthesized with these linkers lack open coordination sites and the frameworks are typically hydrophobic. Linear bispyrazolate[67] and square tetrapyrazolate[122] linkers paired with $Ni_8(OH)_4(H_2O)_2$ SBUs can result in exceptionally stable MOFs that are also highly hydrophobic, absorbing water only above 80% RH in one case.[123] The hydrophilicity of pyrazolate frameworks can be modulated via organic linker modification, though these modifications can reduce the overall water capacity, as they occupy space in the pore, and can also result in broadening of the water uptake step (see also above).[48]

MOFs constructed from linear bistriazolate frameworks contain a high density of open coordination sites, making them very hydrophilic. M_2Cl_2BTDD has a topology similar to that of MOF-74, including hexagonal pores lined with infinite one-dimensional (1D) chains of metal ions exhibiting open coordination sites, and the Co^{2+} and Ni^{2+} analogs are stable to repeated

water uptake.[41] Although the size of its mesopores exceed the critical diameter for water capillary condensation, Co_2Cl_2BTDD reversibly sorbs water without hysteresis due to water coordination at the open metal sites prior to the pore filling step. The smaller pore analog M_2Cl_2BBTA also has been explored for water uptake, and by virtue of its smaller pore size, it is significantly more hydrophilic, capturing water near 0% RH.[43] Among the metal ions tested, Ni_2Cl_2BBTA was found to be most stable, and the stability trend is in line with the metal-aquo substitution rates. Although they form hexagonal structures with the majority of late transition metals, linear bistriazolate linkers form a cubic structure when treated with Zn^{2+}. The resulting framework, $Zn_5Cl_4(BTDD)_3$ (MFU-4*l*),[124,125] has a very large water uptake capacity greater than 1 g g^{-1}. Cation exchange of the native Zn^{2+} material for Co^{2+} enables the modulation of the RH of water uptake over a range of nearly 30%, without decreasing the overall capacity, due to the greater propensity for a tetrahedral Co^{2+} to accept a fifth ligand.[99] However, the cubic BTDD-based frameworks exhibit significantly decreased stability relative to the hexagonal frameworks, with the fully exchanged Co^{2+} material collapsing in the presence of water vapor.[99]

Table 1: Water Capacities for Selected Porous Materials

	α[a] (% RH)	Uptake (g g^{-1})	Crystal ρ (g cm^{-3})	Uptake (cm^3 cm^{-3})
Co_2Cl_2BTDD[41]	29	0.97	0.65	0.6305
Cr-*soc*-MOF[73]	75	1.95	0.381	0.74295
Cr-MIL-101[97]	43	1.6	0.48	0.768
MOF-841[58]	22	0.51	1.05	0.5355
MOF-801[58]	9	0.28	1.59	0.4452
Ni_2Cl_2BBTA[43]	3	0.4	1.1	0.44
Cr-*acs*-MOF[120]	48	1.09	0.539	0.58751
CAU-10[112]	18	0.38	1.15	0.437
MIL-160[115]	8	0.37	1.15	0.4255
MOF-303[94]	15	0.48	1.159	0.55632
Ti-MIL-125-NH_2[121]	23	0.68	0.757	0.51476
Al fumarate[89]	28	0.45	1.24	0.558
MIP-200[107]	18	0.45	1.16	0.522
UiO-66[89]	34	0.43	1.24	0.5332
Ni_8(L3)[123]	40	0.99	0.69	0.6831
Ni_8(L5)[123]	70	1.12	0.64	0.7168
Zn-MFU4*l*[99]	65	1.04	0.58	0.6032
Zn_2Co_3-MFU4*l*[99]	40	1.11	0.58	0.6438
NU-1000[89]	75	1	0.486	0.486
ALPO-78[126]	18	0.32	1.7	0.544
AQSOA Z02[89]	8	0.3	1.43	0.429
AQSOA Z01[89]	17	0.18	1.75	0.315
AQSOA Z05[89]	25	0.18	1.75	0.315

[a]α is the %RH at which half of the total uptake is reached

NH_3

Occurrence, Applications:

Ammonia is an industrial gas produced on a massive scale, whose toxicity has prompted significant research focused on its detection and sensing[127–129] as well as personal protection and mitigation.[130–133] To reduce the ammonia concentration below the NIOSH immediate danger threshold (300 ppm)[134] or below the odor threshold of 5 ppm,[135] sorbents must have a high affinity for ammonia at low relative pressure. Research in materials for personal protection has not focused substantially on framework stability because single-use sorbents that could collapse on contact with ammonia are acceptable under certain conditions. However, stability remains somewhat important as pore collapse during use can substantially impact the performance of a protective sorbent. Other applications may require extensive NH_3 cycling stability. For instance, ammonia is a common impurity in feed gas streams which may poison catalysts and membranes, necessitating the use of sorbents to capture NH_3 prior to the desired chemical process. Finally, on a thermodynamic basis NH_3 is an excellent working fluid for heat transfer in adsorption heat pumps, which require many thousands of adsorption cycles and materials with extreme stability to this corrosive gas.[89]

MOF sorbents for NH_3:

In order to capture NH_3 at low relative pressure, one commonly employed strategy is the use of MOFs exhibiting Lewis acidic open metal sites, including HKUST-1, MOF-74, and M_2Cl_2BBTA frameworks. For example, HKUST-1 exhibits a high capacity for ammonia of 12.1 mmol g^{-1} at 1 bar[136] but loses crystallinity upon ammonia exposure in under two hours.[137] According to NMR data, the reaction of HKUST-1 with anhydrous ammonia produces a diamine copper complex with a pendant anionic trimesate ligand. In the presence of water, the product is $Cu(OH)_2$ and $(NH_4)_3$BTC.[75] A polyvinylidene difluoride (PVDF) coating was found to protect HKUST-1 from ammonia; the composite maintained crystallinity as well as a constant NH_3 capacity over 28 days.[138] Analogs of MOF-74 have high capacities for ammonia based on breakthrough measurements, with the champion Mg^{2+} material able to capture 7.6 mmol g^{-1} NH_3 before breakthrough, although the presence of water substantially decreased the uptake.[139] In a separate study, Cu-MOF-74 was found to take up more ammonia with water vapor present, though the material was unstable to ammonia.[140]

Employing more donating triazolate linkers, M_2Cl_2BTDD materials were the first examples of MOFs exhibiting a high density of open metal sites stable to repeated sorption and desorption of ammonia.[40] The Ni^{2+} analog is stable to complete pore filling with ammonia, which occurs in a stepwise fashion near 0.8 bar of pure NH_3 at 263 K.[42] Due to their greater density of open coordination sites, the smaller-pore M_2Cl_2BBTA materials capture significantly more ammonia, particularly at low pressures. The Cu^{2+} analog has the greatest static capacity at 1 bar and 298 K of any MOF, but it is unstable to even low concentrations of NH_3, which compromises its dynamic breakthrough performance. The cobalt material, though it loses crystallinity at 1 bar of ammonia, is stable to 1 mbar NH_3, the conditions of a typical breakthrough test. This enables M_2Cl_2BBTA to capture the greatest quantity of ammonia of any material under dry breakthrough conditions. The nickel material is significantly more stable, and the stability trend based on the NH_3 pressure required to effect loss of crystallinity and porosity in this family of triazolate MOFs is once again in line with that expected based on the substitution kinetics of the metal ion hexaaquo complexes.[42]

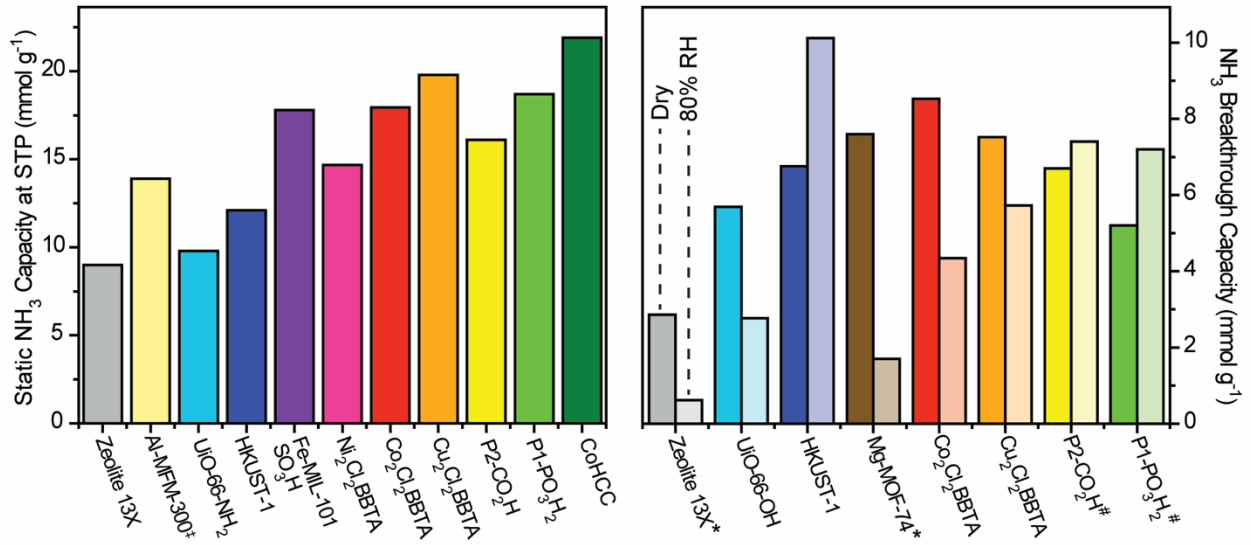

Figure 5: **Ammonia Capacities of Porous Solids.** Left: NH_3 capacity at 1 bar, 298 K based on equilibrium isotherm data. ‡Tested at 293 K. Right: NH_3 capacity under dynamic breakthrough conditions at 1000 ppm, 298 K in both dry and humid conditions. Tested at *1440, #2880 ppm. Values and references listed in **Tables 2** and **3**.

MOFs without open coordination sites have also been investigated for ammonia capture. In order to enhance the affinity for NH_3, ligand functionalization with polar or acidic groups is commonly employed. For instance, amino-functionalized MOF-5 has a high capacity for ammonia, sorbing 6.2 mmol g^{-1} in breakthrough testing in a stream 1% NH_3, exceeding the capacity of Zn-MOF-74.[141] Composites of graphene oxide with MOF-5 can also enhance ammonia uptake, though the framework collapses rapidly in the presence of NH_3.[142] Zn^{2+} frameworks isoreticular to MOF-5 featuring ligands with free -OH groups can capture up to 16.4 mmol g^{-1} NH_3 in static measurements at STP, though with loss of surface area and crystallinity.[143]

The Zr^{4+} carboxylate framework UiO-66 has been extensively investigated for ammonia capture, and a diverse array of organic functional groups have been explored to enhance the affinity for NH_3.[84] Amino-functionalized UiO-66 outperforms derivatives with more acidic but bulkier functional groups such as -COOH and -SO_3H in breakthrough measurements, presumably due to pore clogging effects with larger moeities.[144] Similarly, the addition of copper sites to pendant free carboxylates can enhance equilibrium NH_3 uptake at the expense of diffusion.[145] Further investigation of UiO-66-NH_2 revealed that a portion of the amino groups may be protonated -NH_3Cl groups under typical acidic synthesis conditions, and that further functionalization to the hemiaminal or aziridine can enhance NH_3 capacity.[146] Although stable to short exposure times,[137] repeated cycling of ammonia uptake in UiO-66-NH_2 revealed a loss of capacity, surface area and crystallinity.[40]

Trivalent Cr^{3+}, Al^{3+}, and Fe^{3+} carboxylate frameworks can exhibit increased stability toward ammonia,[137] though they have not been widely explored as sorbents. A framework comprised of Al^{3+} and a biphenyl tetracarboxylate linker, termed Al-MFM-300, was stable for 50 cycles of ammonia uptake with a high static capacity of 13.9 mmol g^{-1} at 1 bar.[147] Additionally, a highly stable Al^{3+} porphyrin MOF can be loaded with HCl or formic acid to achieve up to 7.9 wt% breakthrough capacity.[148] Further, Fe^{3+}-MIL-101 functionalized with sulfonic acid groups captures 17.8 mmol g^{-1} NH_3 at STP, and has a high affinity for ammonia at low pressure.[149]

Other families of porous materials have recently been investigated for ammonia capture. All-inorganic Prussian blue analogs, by virtue of their exceptional density of Lewis acidic metal sites, have particularly high static capacities for NH_3 of over 20 mmol g^{-1} and can be regenerated.[150] Further, more recent covalent organic frameworks (COFs) with more robust linkages may find utility in ammonia sorption. Thus, although boronate ester-linked COF-10 can capture 15 mmol g^{-1} NH_3 at STP, slow degradation was observed with cycling as the linkages remain susceptible to nucleophilic attack.[151] On the other hand, porous polymers with all-carbon backbones such as diamondoid structures densely functionalized with acidic groups can exhibit superlative capacity and stability for NH_3, with uptake of 18.7 mmol g^{-1} NH_3 at STP for the phosphonic acid functionalized material, although diffusion is compromised due to their interpenetrated nature.[149,152]

Table 2: Equilibrium Ammonia Capacities at 1 bar, 298 K for Selected Porous Materials

	NH_3 Capacity (mmol g^{-1})
Zeolite 13X[147]	9
Amberlyst 15[147]	11
MCM-41[147]	7.9
UiO-66-NH_2[40]	10.6
HKUST-1[136]	12.1
DUT-6[143]	12
DUT-6-$(OH)_2$[143]	16.4
Fe-MIL-101-SO_3H[149]	17.8
Al-MFM-300[147]	13.9
P1-PO_3H_2[152]	18.7
P2-CO_2H[152]	16.1
Mn_2Cl_2(BTDD)[40]	15.47
Co_2Cl_2(BTDD)[40]	12
Ni_2Cl_2(BTDD)[40]	12.02
Cu_2Cl_2(BTDD)[42]	16.74
Co_2Cl_2(BBTA)[42]	17.95
Ni_2Cl_2(BBTA)[42]	14.68
Cu_2Cl_2(BBTA)[42]	19.79
Al-MFM-300[147]	13.9
Prussian blue[150]	12.5
CoHCC[150]	21.9
CuHCF[150]	20.2
$MgCl_2$[153]	54.8

Table 3: Breakthrough NH_3 Capacities for Selected Porous Materials

	ppm NH_3	**Dry (mmol g^{-1})**	**Humid (80% RH) (mmol g^{-1})**
UiO-66-OH[144]	2880	5.69	2.77
Zeolite 13X[139]	1440	2.86	0.62

P1-PO_3H_2[152]	2880	5.2	7.2
P2-CO_2H[152]	2880	6.7	7.4
HKUST-1[154]	1000	6.76	10.12
Mg-MOF-74[139]	1440	7.6	1.7
Co_2Cl_2BTDD[42]	1000	4.75	3.37
Co_2Cl_2BBTA[42]	1000	8.53	4.34
Cu_2Cl_2BTDD[42]	1000	7.52	5.73

H_2S

Occurrence, Applications:

Hydrogen sulfide is a major contaminant in flue gas streams as well as in many sources of natural gas, termed sour gas. When present in process streams it can poison catalysts, corrode components, and if not removed, combust into SO_x, a major air pollutant. Additionally, H_2S is highly toxic and heavier than air, making personal protection and mitigation vital to reduce the concentration below the OSHA exposure limit of 10 ppm, or the odor threshold of 1.5 ppm.[135,155] The detection[156–158] and removal of H_2S is therefore of great interest, and limited research in the MOF community has focused on these applications.

MOF sorbents for H_2S:

MOFs with open metal sites have been explored to capture H_2S, including HKUST-1, which exhibits a high capacity, though as with NH_3, the framework is unstable to H_2S. Partial protonation of the trimesate ligand by H_2S is proposed to result in framework collapse, although formation of CuS may also drive decomposition in this case. Similar to their performance with NH_3, HKUST composites with graphene oxide capture more H_2S than the parent materials, but suffer from similar stability issues.[159,160] The use of non-structural metal ions with open coordination sites can provide strong binding sites for H_2S while also maintaining framework stability. Employing UiO-67-bipyridine grafted with Cu^{2+} gives a high capacity for H_2S of up to 7.8 wt%, on par with the 8 wt% in the comparatively unstable HKUST-1.[161]

High-valent metal terephthalates including Zr-UiO-66, Cr-MIL-101 and Ti-MIL-125 as well as their amino-functionalized derivatives were investigated for H_2S capture from natural gas. Of the materials tested, amino-functionalized derivatives performed better, and Ti-MIL-125-NH_2 was the top performer. H_2S was preferentially absorbed over CO_2, though the addition of CO_2 did decrease capacities for H_2S. Cr-MIL-101 performed best with CO_2 present.[162] Additionally, V-MIL-47 and Cr-MIL-53 were investigated for H_2S capture at high pressures. Both V and Cr materials appear to be stable up to 15 bar H_2S, whereas Fe-MIL-53 decomposes under similar conditions to what is likely iron sulfide and H_2BDC.[32]

Select pyridinic MOFs with relatively inert divalent metal ions can withstand H_2S exposure. For example, $Mg_3(OH)_2$(2,4-pyridine dicarboxylate)$_2$ (Mg-CUK-1), captures more than 3 mmol H_2S g^{-1} when exposed to 15% H_2S in nitrogen, and the material remained stable over five cycles.[163] Additionally, Ni^{2+}-pyrazine (py) frameworks employing anionic inorganic pillars can absorb both CO_2 and H_2S from natural gas streams,[164] and were investigated for H_2S separations using mixed-matrix membranes. The Ni^{2+}-based $NbOF_5^{2-}$ and AlF_5^{2-}-pillared materials[165] significantly increase both the selectivity and the permeability of the host polymer membrane for H_2S, and both materials remain stable by PXRD after exposure to 14 bar H_2S.[166]

The Ni^{2+} materials are more stable to H_2S, as well as to water, than analogous Cu^{2+} frameworks employing SiF_6^{2-} as the pillar, with Ni(py)(AlF_5) stable to 15 cycles of water uptake.[167,168]

MOFs employing more strongly donating azolate ligands have not been widely explored for H_2S capture. Notwithstanding, Zn(tetrazolate) (*kag*-MOF-1), which is stable to water and low concentrations of H_2S, selectively absorbs H_2S over higher hydrocarbons due to its small pore diameter.[169]

SO_2

Occurrence, Applications

Sulfur dioxide is a major air pollutant generated by combustion of sulfur-containing materials including coal, sour natural gas, or metal sulfide ores. SO_2 is a significant contributor to the formation of acid rain and fine particulate matter ($PM_{2.5}$), making the capture of SO_2 from exhaust gases vital. In North America, SO_2 emissions have decreased by 90% over the past 20 years[170] because of the implementation of SO_2 removal technologies, including dry limestone scrubbing and the wet sulfuric acid process,[171] yet these processes are not 100% efficient. As a result, coal-fired power plants continue to emit 1.2 million tons yr^{-1} of SO_2 in the USA alone.[172] In addition to the environmental benefits of reducing SO_2 emissions, the complete removal of SO_2 is often critical prior to contact with downstream catalysts or adsorbent materials intended for other gases.[173,174] Consequently, new adsorbent materials that remove SO_2 at low partial pressure are attractive targets in post-combustion exhaust capture, an application which would require extensive cycling stability under humid conditions. Here, we cover standout examples of MOF stability towards SO_2, as recent reviews provide detailed coverage.[175]

MOFs for SO_2 Adsorption

Metal-carboxylate MOFs

Tetravalent metal carboxylate frameworks can exhibit high uptake capacities for SO_2. For instance, the eight-connected Zr^{4+} material MFM-601, $[Zr_6(\mu^3\text{-}O)_4(\mu^3\text{-}OH)_4(OH)_4(H_2O)_4(L)_2]$ (L =4,4′,4″,4‴-(1,4-Phenylenebis(pyridine-4,2,6-triyl))tetrabenzoate), adsorbs 12.3 mmol g^{-1} SO_2 at STP. In-situ powder X-ray diffraction revealed six binding sites, the strongest of which is adjacent to a terminal hydroxyl group at the node. Adsorption properties under humid conditions have not been reported. Moving to Ti^{4+} frameworks, Ti-MIL-125 has a high uptake capacity under anhydrous conditions of 10.9 mmol g^{-1} at 2.6 bar, but decomposes under humid SO_2.[176] By contrast, the addition of an -NH_2 group to the linker stabilizes the framework under humid conditions, and Ti-MIL-125-NH_2 retains a comparable SO_2 adsorption capacity of 10.3 mmol g^{-1} at 2.6 bar. Decomposition in Ti-MIL-125 was proposed to result from hydrolysis of the metal ligand bond, followed by reaction with SO_2 to form bisulfite (HSO_3^-) and a dangling linker. Calculations reveal that in Ti-MIL-125-NH_2, the activation energy barrier for hydrolysis of the Ti-O bond is augmented by ~5 kcal mol^{-1} which engenders enough additional stabilization to sufficiently slow the decomposition pathway.[176]

Initial results show that trivalent Al^{3+} and In^{3+} carboxylate frameworks reversibly bind dry SO_2 in static adsorption experiments.[177–179] The Al^{3+} carboxylate MOFs, MFM-305-CH_3, MFM-305, and MFM-300 (née NOTT-300) all reversibly adsorb SO_2 with high capacities above 5 mmol g^{-1}.[178,179] In situ powder X-ray diffraction analysis on MFM-300 revealed that SO_2 strongly interacts with the bridging hydroxyl groups of the SBU.[178] Moving to the more labile In^{3+}, NOTT-202a $[In(O_2CR)_4]$ (O_2CR = biphenyl-3,3,5,5-tetra-(phenyl-4-carboxylate)) reversibly binds SO_2 with an adsorption capacity of 10 mmol g^{-1} at 1 bar and temperatures between 293–

303 K.[177] However, low temperature (268–283 K) SO_2 adsorption isotherms feature hysteretic adsorption of an additional 2-6 mmol SO_2 g^{-1} as a consequence of an irreversible phase change to form a denser crystalline polymorph. Despite the phase change, SO_2 is completely removed from NOTT-202b at zero pressure, suggesting that SO_2 does not react directly with the framework. It was suggested that the phase change in NOTT-202a occurs due to ordering of SO_2 within the pore at adsorption capacities greater than 7 mmol g^{-1} SO_2, similar to a pore condensation phenomenon, and the internal pressure thus created provides enough energy to overcome the activation barrier to transform to the denser NOTT-202b, which is 20 kJ mol^{-1} downhill in energy due to increased ligand pi-stacking.

Late transition metal-carboxylate frameworks exhibit poorer stability towards SO_2. Dynamic breakthrough measurements of MOF-5, IRMOF-3, Zn-MOF-74, MOF-177, and MOF-199, all Zn^{2+}-based, revealed uptake capacities of less than 0.5 mmol g^{-1} for all materials except MOF-74, which adsorbs 3.0 mmol g^{-1} presumably due to its open metal sites.[180] Increased stability towards dry SO_2 in pillared Zn^{2+} carboxylate MOFs can be achieved by either increasing the steric bulk on the linker, or by replacing Zn^{2+} with the more inert Ni^{2+}.[76,181]

Pyridinic coordination networks SIFSIX-1-Cu and SIFSIX-2-Cu-i can exhibit high and stable uptakes to dry SO_2. Consisting of square grids of Cu^{2+} and 4,4'-bipyridine or 4,4'-dipyridylacetylene pillared by SiF_6^{2-} anions, these frameworks exhibit dry SO_2 adsorption capacities of 11.01 and 6.90 mmol g^{-1}, respectively. Replacing Cu^{2+} with Zn^{2+} or Ni^{2+} results in lower capacities of 2.10 and 2.74 mmol g^{-1}, respectively. The materials were stable to dry breakthrough testing over 4-6 cycles with mild reactivation parameters of 313 K and He flow, though humid stability above 1000 ppm H_2O was not evaluated.[182] Additionally, the pyridinic frameworks $Ni(py)_2(NbOF_5)$ and $Ni(py)_2(AlF_5)$ both exhibit dry uptakes of 2.2 mmol g^{-1} when exposed to 7% SO_2 in N_2.[183] Moreover, these materials exhibit stability towards SO_2 under humid environments.

Metal-Azolate MOFs

To date, few metal azolate frameworks have been explored for SO_2 sorption. One exception is a series of nickel pyrazolate MOFs based on $(Ni_8(OH)_4(H_2O)_2(BDP)_6)$, which show good stability towards SO_2.[184] Dynamic adsorption experiments revealed that the unfunctionalized framework has an SO_2 adsorption capacity of 2.0 mmol g^{-1} under 2.5% SO_2 in N_2. The addition of amino or hydroxyl functional groups to the BDP ligand, as well as treatment with Bronsted bases to augment the defect concentration, both result in enhanced SO_2 capacity (**Table 4**). Within this family of Ni^{2+} pyrazolate MOFs, SO_2 binding was not completely reversible: cycling experiments revealed a decrease of 26-37% capacity after the first cycle. However, the decay appeared to stop after the first cycle, and the remaining SO_2 capacity in the second cycle appeared to be reversible. The initial decrease in capacity was attributed to the irreversible formation of bisulfite ($M\text{-}SO_3H$) or sulfite ($M\text{-}SO_3(H_2O)$) at the node.

Although no sorption was reported, the stability of several ZIFs under dry and humid SO_2 conditions has been explored.[185] A negligible ~4% decrease in the surface area of ZIF-8 was observed after exposure to dry SO_2, however, the surface area decreases by ~70% after exposure to 20 ppm SO_2 at 85% RH over 10 days. Similar loss of porosity was observed for other ZIFs, except for ZIF-71 ($Zn(4,5\text{-dichloroimidazolate})_2$), which retained its full pore volume, though curiously, it transitions to a dense polymorph in liquid water. Analysis by X-ray photoelectron spectroscopy (XPS) and infrared (IR) spectroscopy revealed formation of bisulfite and bisulfate, presumably resulting from metal-ligand bond hydrolysis, within the ZIFs which lost porosity.[185]

Table 4: Static SO_2 Capacities at 1 bar, 298 K for select MOFs.

	SO_2 Capacity (mmol g^{-1})
MFM-601[186]	12.3
MFM-600[186]	5.0
MFM-202a[177]	10
Ni(bdc)(ted)$_{0.5}$[181]	9.97
Zn(bdc)(ted)$_{0.5}$[181]	4.41
MOF-74(Mg)[181]	8.60
MFM-300(Al)[178+] **(NOTT-300)**	8.1
MFM-300(In)[187]	8.3
Zn-DMOF-TM[a][76]	~4.5 (dry)
Zn-DMOF-DM[b][76]	degrades
Zn-DMOF-NDC[c][76]	~4 (dry)
Zn-DMOF-ADC[d][76]	~5.5 (dry)
Cu-DMOF-TM[a][76]	~2.8 (dry)
Ni-DMOF-TM[a][76]	~5 (dry)
Co-DMOF-TM[a][76]	~3.8 (dry)
FMOF-2[188]	1.8
MFM-305-CH_3[179]	5.16
MFM-305[179]	6.99
SIFSIX-1-Cu[182]	11.01
SIFSIX-2-Cu-i[182]	6.9
MIL-125[176]	~9.5
MIL-125-NH_2[176]	~9.5

[a]TM – tetramethylterephthalic acid, [b]DM – 2,5-dimethyl terephthalic acid, [c]NDC – 1,4-naphthalenedicarboxylic acid, [d]ADC – 9,10-anthracenedicarboxylic acid. [e]250 ppm with days long exposure to SO_2. [+]Measured at 273 K

Table 5: Dynamic SO_2 Capacities for select MOFs.

	ppm SO_2	SO_2 Capacity (mmol g^{-1})
MOF-5[180]	pure	<0.02

IRMOF-3[180]	pure	0.94
Zn-MOF-74[180]	pure	3.03
MOF-177[180]	pure	<0.02
MOF-199[180]	pure	0.50
IRMOF-62[180]	pure	<0.02
Co-MOF-74[139]	382	0.63 (dry) 0.03 (humid)
Mg-MOF-74[139]	382	1.60 (dry) 0.72 (humid)
Ni-MOF-74[139]	382	0.04 (dry) 0.02 (humid)
Zn-MOF-74[139]	382	0.26 (dry) 0.04 (humid)
$[Ni_8(OH)_4(H_2O)_2(BPD\_H)_6]$[184]	25000	2.02
$[Ni_8(OH)_4(H_2O)_2(BPD\_OH)_6]$[184]	25000	2.11
$[Ni_8(OH)_4(H_2O)_2(BPD\_NH_2)_6]$[184]	25000	3.35
$K[Ni_8(OH)_3\ (EtO)_3(BDP\_H)_{5.5}]$[184]	25000	3.26
$K_3[Ni_8(OH)_3\ (EtO)(BDP\_O)_5]$[184]	25000	2.54
$K[Ni_8(OH)_3\ (EtO)_3(BDP\_NH_2)_{5.5}]$[184]	25000	4.38
$Ba_{0.5}[Ni_8(OH)_3(EtO)_3(BDP\_H)_{5.5}]$[184]	25000	4.0
$Ba_{1.5}[Ni_8(OH)_3\ (EtO)(BDP\_O)_5]$[184]	25000	3.65
$Ba_{0.5}[Ni_8(OH)_3(EtO)_3(BDP\_NH_2)_{5.5}]$[184]	25000	5.61
$Ni^{II}_2\{Ni^{II}_4[Cu^{II}_2\text{-}(Me_3mpba)_2]_3\}$[189]	25000	2.0
$Ba^{II}_2(H_2O)_9\{Ni^{II}_4[Cu^{II}_2\text{-}(Me_3mpba)_2]_3\}$[189]	25000	2.5

NO_x

Occurrence, Applications

The major components of nitrogen oxides (NO_x) are nitrogen monoxide (NO) and nitrogen dioxide (NO_2). These highly toxic species are damaging to respiratory health and contribute to environmental pollution in the troposphere (photochemical smog) and stratosphere (ozone depletion). Anthropogenic NO_x sources are approximately split between agriculture and combustion processes in power plants and automobiles.[190] Given their detrimental effects to health and the environment, NO_x emissions are highly regulated, and recently, more stringent regulations are further incentivizing capture or mitigation of NO_x prior to release.[191] Current exhaust systems use catalytic converters to reduce NO_x to N_2 and H_2O, and some MOFs have been investigated for this application,[192–195] but to achieve further reductions, for instance, during cold engine starting, the exhaust systems of combustion engines require added technologies that can adsorb NO or convert NO_x into environmentally benign species. The composition of NO_x

from an exhaust engine varies depending on the fuel source, yet the majority of NO_x is initially composed of NO.[196]

Somewhat counterintuitively given its toxicity, NO plays a signaling role in many critical physiological processes, such as vasodilation, immune defense, and neuronal signal transduction.[197] The therapeutic properties of NO have motivated efforts to design materials which release NO under specific biologically-relevant conditions.[198,199]

MOFs for NO Adsorption

Adsorption of NO predominantly occurs in MOFs exhibiting open metal sites. For instance, HKUST-1 adsorbs 9 mmol NO g^{-1} MOF at 1 bar and 196 K.[200] NO interacts directly with the metal, as evidenced by the ν(NO) band at 1887 cm^{-1}, comparable to IR bands of Cu^{2+}-NO in molecular complexes[201] and zeolites.[202] Exposure of NO-loaded HKUST-1 to a flow of humid air resulted in minor release of NO (2 μmol g^{-1}), and the material lost crystallinity after NO release. The incorporation of amino-functionalized trimesic acid linkers into HKUST-1 improved the quantity of NO released, but the stability remained poor.[203]

$Fe_3O(OH)(BDC)_3$ (Fe-MIL-88) and a series of functionalized derivatives adsorb between 1 and 2.5 mmol NO g^{-1} MOF with no loss of crystallinity.[204] For therapeutic applications, only 5-14% of NO was released upon exposure to humid conditions, and it was noted that most of the NO was likely released prior to the measurement run, suggesting that these materials do not bind NO tightly enough to be stable for long term storage.[204]

The high density of open metal sites in the MOF-74 series make them attractive for NO sorption studies. The Co^{2+} and Ni^{2+} derivatives each adsorb ~7 mmol NO g^{-1}, and can be stored with NO bound for several months under inert conditions, making them attractive for medical therapies. Flowing humid air through the MOFs results in complete recovery of the starting material.[205,206] The biocompatible Mg^{2+} and Zn^{2+} MOF-74 analogs have also been investigated for NO adsorption/desorption. Mg-MOF-74 binds NO too strongly and does not release NO under 11% RH conditions, whereas Zn-MOF-74 loses NO too readily under preparatory conditions. However, by doping Mg-MOF-74 with up to 40% Ni^{2+}, the quantity and rate of deliverable NO can be tuned.[207] Moving to NO-loaded Fe-MOF-74, gradual release of NO occurs under a flow of 11% RH.[208] Additionally, the Fe material adsorbs 6.21 mmol NO g^{-1} MOF at 7 mbar, corresponding to 95% occupation of the Fe^{2+} open metals sites by NO.[208]

MOFs for NO_2 Adsorption

There are only limited reports of NO_2 adsorption in MOFs. The Zr^{4+} carboxylate frameworks UiO-66 and UiO-67 capture 7.3 wt% and 7.9 wt% NO_2, respectively, under 1000 ppm dry NO_2, and the capacity of UiO-67 was further augmented to 11.8 wt% under 71% RH, presumably due to NO_2 dissolution into pore-confined water. Further, amino-functionalization of the linker of UiO-66 resulted in a nearly fivefold improvement in the static NO_2 capacity.[209,210] However, IR and NMR spectroscopy revealed evidence of amine diazotization as well as nitrosation of the phenyl C–H bonds, revealing the complex reaction pathways possible upon NO_2 adsorption.[210] Indeed, NO_2 adsorption is not reversible in UiO-66-type frameworks, and it was proposed that NO_2 reacts at the Zr–O–Zr bridges resulting in partial framework collapse.[209]

Reversible NO_2 capture was achieved in the Al^{3+} carboxylate MOF, MFM-300, which adsorbs 14.1 mmol NO_2 g^{-1} MOF over five cycles with no loss in capacity or crystallinity. Analysis of an NO_2 loaded sample using synchrotron powder x-ray diffraction revealed a 1D helical chain of NO_2 and N_2O_4 units within the pores. Each NO_2 forms five distinct weak

interactions with the framework, a consequence of the precisely tailored pore size providing stabilization for the helical chain. Additionally, the material exhibits preferential binding of NO_2 over CO_2 and SO_2. Notably, under wet conditions (0.5% NO_2 in N_2) the NO_2 breakthrough time decreases by ~10% compared to dry conditions, a decline postulated to result from competitive binding between H_2O and NO_2. Analysis of the material post-breakthrough experiment was not detailed.[211]

Leveraging the chemistries of the daughter products of NO_2 reactivity, the addition of NO_2 to a Zr^{4+} carboxylate MOF featuring a calixarene linker results in partial formation of N_2O_4, leading to the disproportionation products NO^+ and NO_3^-. The resulting NO^+ transfers to the calixarene linker, generating a strongly adsorbed donor-acceptor complex detected using calorimetry. Interestingly, the process appears to be reversible and the material retained crystallinity after repeated NO_2 exposure.[212]

Halogens

Occurrence, Applications

Most research on the adsorption of halogens by metal-organic frameworks has focused on I_2, which is motivated by the capture of volatile radioisotopes of I_2 from nuclear waste streams.[213–220] Here, we focus on the more volatile lighter halogens Cl_2 and Br_2, which are much less commonly explored even though the capture and reversible storage of the highly toxic halogen elemental gases is of great interest to improve personal protective equipment, as well as to more safely handle, store, and transport X_2.

MOFs for X_2 Adsorption

Unfunctionalized carboxylate frameworks, including MOF-5, UiO-66, and Al-MIL-53, exhibit negligible Cl_2 uptake under dynamic conditions. Addition of an -NH_2 group to the terephthalate linker greatly enhances the irreversible Cl_2 uptake, to 35.5 wt% in the case of MOF-5-NH_2.[180] Similarly, both UiO-66-NH_2 (154 wt%) and Al-MIL-53-NH_2 (56 wt%) have orders of magnitude larger Cl_2 uptakes than their parent materials UiO-66 (3 wt%) and MIL-53 (1 wt%).[221] By contrast, functionalization with a hydroxy group in the case of UiO-66-OH (5 wt%), does not significantly improve chlorine uptake. Mechanistically, these enhancements are due to the amino groups, which promote electrophilic aromatic substitutions in positions ortho to themselves, resulting in a chlorinated ring and -NH_3Cl. Clearly, this is an irreversible process that cannot be utilized cyclically.

Reversible storage of the lighter halogens was demonstrated using Co_2Cl_2(BTDD).[222] The cobalt metal centers are redox-active and feature an accessible Co(II/III) redox couple suitable for reactions with Cl_2 and Br_2. Exposure of Co_2Cl_2(BTDD) to either of the two elemental halogens results in the oxidation of five-coordinate Co^{2+} to octahedral Co^{3+}, forming $Co_2Cl_2X_2$(BTDD) (X = Cl or Br), while maintaining crystallinity and porosity (**Figure 7**). Heating the Co^{3+} material to 275 °C (X = Cl) or 195 °C (X = Br), results in the reductive release of X_2 gas, and reformation of the parent Co_2Cl_2(BTDD). The capture and release of Br_2 was repeated over three cycles with reproducible yields of 75–80% on the initial cycle and 100% yield on subsequent ones.[222] The exceptional stability of Co_2Cl_2(BTDD) towards X_2 is attributed to strong M–L bonds, open metal sites with an accessible Co(II/III) redox couple, and particularly strong aromatic C–H bonds that are not susceptible to radical X· attack. Indeed, after oxidation, the framework stability may increase due to the eight orders of magnitude slower rate of ligand exchange for Co^{3+} as compared to Co^{2+}.

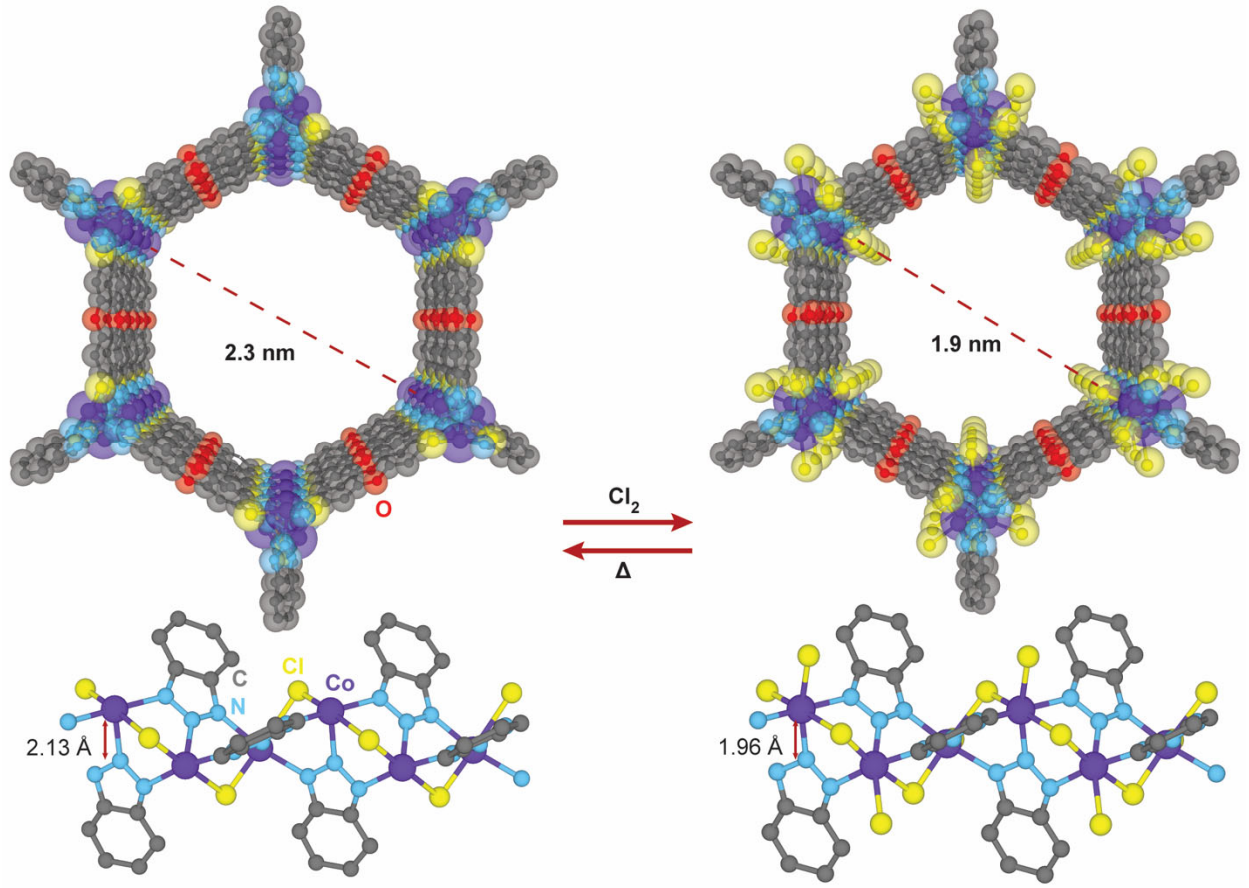

Figure 6: **Oxidative Capture of X_2.** Co_2Cl_2BTDD captures Cl_2 (or Br_2) via reversible oxidation to Co_2Cl_4BTDD (or $Co_2Cl_2Br_2BTDD$). H atoms omitted for clarity.

Conclusions and Outlook

It is frequently cost-prohibitive to remove all H_2O, NH_3, H_2S, or SO_x/NO_x from the atmosphere or from feed gas streams. Therefore, the use of MOFs in applications such as CO_2 removal from flue gas requires long-term stability to coordinating and corrosive species. Additionally, although we have divided this review into separate sections containing each analyte gas, these species are often present together, which may present other challenges, such as the formation of H_2SO_4 from SO_x, water, and oxygen. Multicomponent stability testing has largely been overlooked thus far, but it is vital. The design of frameworks for the capture of these challenging gases pushes the boundaries of sorbent robustness and advances our understanding of the fundamental kinetics and thermodynamics of MOF stability.

MOFs are most often synthesized from weakly donating ligands, such as carboxylates, in combination with labile metal ions such as Zn^{2+} and Cu^{2+}. Together, these favor reversible ligand binding to promote ideal crystal growth. The crystallization of MOFs using inert metal ions, such as Cr^{3+}, or more strongly donating ligands, such as pyrazolates, is more difficult because the reversible sampling of configurations towards the local minimum energy state is not as efficient. Therefore, harsh synthetic conditions such as high temperature, high pressure, and the use of mineralizers such as HF are often required.[30] Consequently, it becomes more difficult to obtain large crystals, which may complicate structure determination. Indeed, the structures in original reports of Cr-MIL-53 and Cr-MIL-101 were solved using powder refinement rather than by more

straightforward single-crystal methods which require larger cystals.[30,31] Although the synthesis of MOFs containing inert metals, or ligands that are more strongly donating, can be challenging,[223,224] it may lead to structures capable of withstanding demanding conditions relevant for many applications, such as gas storage and separations involving impure gas streams containing water vapor, ammonia, or acid gases. Ultimately, nothing good comes easy. By and large, MOFs that crystallize very easily and grow as large single crystals tend to be less stable to water or other corrosive and coordinating gases.

Porous materials are kinetically stable. Currently, the default vocabulary for describing the stability of MOFs is a binary scale: stable versus unstable. Moving forward, our view is that MOFs will be ranked on a continuum of kinetic stability. Quantitative benchmarking of all MOFs using a broadly applicable stability rating, such as those already employed using water vapor or steam temperature,[50,225] could significantly advance the field. Recent research has followed two main paths to stabilize the porous phase, either by engineering heterolytically stronger metal ligand bonds, or by using more inert metals. This has led to exceptionally robust frameworks, and portends the use of MOFs for applications requiring extensive stability toward harsh gases and vapors, as well as in areas requiring long-term lower level stability. Future progress in this direction will enable MOFs to fulfill their promise as designer multifunctional materials for diverse applications.

Acknowledgements
Studies of small molecule interactions with metal nodes in MOFs are supported through a CAREER grant from the National Science Foundation to M.D. (DMR-1452612). A.J.R. is supported by the Martin Family Fellowship for Sustainability. We thank the Abdul Latif Jameel World Water and Food Security Lab for seed funding for water capture.

Competing Interests Statement
The authors declare no competing interests

References
1. Furukawa, H., Cordova, K. E., O'Keeffe, M. & Yaghi, O. M. The Chemistry and Applications of Metal-Organic Frameworks. *Science* **341,** 1230444–1230444 (2013).
2. Mason, J. A., Veenstra, M. & Long, J. R. Evaluating metal-organic frameworks for natural gas storage. *Chemical Science* **5,** 32–51 (2014).
3. Murray, L. J., Dincă, M. & Long, J. R. Hydrogen storage in metal-organic frameworks. *Chem. Soc. Rev.* **38,** 1294–1314 (2009).
4. DeSantis, D. *et al.* Techno-economic Analysis of Metal–Organic Frameworks for Hydrogen and Natural Gas Storage. *Energy & Fuels* **31,** 2024–2032 (2017).
5. Yoon, J. W. *et al.* Selective nitrogen capture by porous hybrid materials containing accessible transition metal ion sites. *Nat. Mater.* **16,** 526–531 (2017).
6. Kizzie, A. C., Wong-Foy, A. G. & Matzger, A. J. Effect of Humidity on the Performance of Microporous Coordination Polymers as Adsorbents for CO 2 Capture. *Langmuir* **27,** 6368–6373 (2011).
7. Adil, K. *et al.* Gas/vapour separation using ultra-microporous metal–organic frameworks: insights into the structure/separation relationship. *Chem. Soc. Rev.* **46,** 3402–3430 (2017).
8. Dusselier, M. & Davis, M. E. Small-Pore Zeolites: Synthesis and Catalysis. *Chem. Rev.* **118,** 5265–5329 (2018).

9. Yang, D. & Gates, B. C. Catalysis by Metal Organic Frameworks: Perspective and Suggestions for Future Research. *ACS Catal.* 1779–1798 (2019). doi:10.1021/acscatal.8b04515
10. Lee, J. *et al.* Metal–organic framework materials as catalysts. *Chem. Soc. Rev.* **38,** 1450–1459 (2009).
11. Sun, L., Campbell, M. G. & Dinca, M. Electrically Conductive Porous Metal – Organic Frameworks Angewandte. *Angew. Chem. Int. Ed.* **55,** 3566–3579 (2016).
12. Hendon, C. H., Rieth, A. J., Korzyński, M. D. & Dincă, M. Grand Challenges and Future Opportunities for Metal-Organic Frameworks. *ACS Cent. Sci.* **3,** 554–563 (2017).
13. Furukawa, H. *et al.* Ultrahigh Porosity in Metal-Organic Frameworks. *Science* **329,** 424–428 (2010).
14. Kitagawa, S. Porous Materials and the Age of Gas. *Angew. Chemie - Int. Ed.* **54,** 10686–10687 (2015).
15. Cheetham, A. K., Kieslich, G. & Yeung, H. H. M. Thermodynamic and Kinetic Effects in the Crystallization of Metal-Organic Frameworks. *Acc. Chem. Res.* **51,** 659–667 (2018).
16. Hughes, J. T. & Navrotsky, A. MOF-5: Enthalpy of Formation and Energy Landscape of Porous Materials. *J. Am. Chem. Soc.* **133,** 9184–9187 (2011).
17. Hughes, J. T., Bennett, T. D., Cheetham, A. K. & Navrotsky, A. Thermochemistry of zeolitic imidazolate frameworks of varying porosity. *J. Am. Chem. Soc.* **135,** 598–601 (2013).
18. Bhunia, M. K., Hughes, J. T., Fettinger, J. C. & Navrotsky, A. Thermochemistry of paddle wheel MOFs: Cu-HKUST-1 and Zn-HKUST-1. *Langmuir* **29,** 8140–8145 (2013).
19. Wu, L., Hughes, J., Moliner, M., Navrotsky, A. & Corma, A. Experimental energetics of large and extra-large pore zeolites: Pure silica beta polymorph C (BEC) and Ge-containing ITQ-33. *Microporous Mesoporous Mater.* **187,** 77–81 (2014).
20. Akimbekov, Z. & Navrotsky, A. Little Thermodynamic Penalty for the Synthesis of Ultraporous Metal Organic Frameworks. *ChemPhysChem* **17,** 468–470 (2016).
21. Akimbekov, Z., Wu, D., Brozek, C. K., Dincă, M. & Navrotsky, A. Thermodynamics of solvent interaction with the metal-organic framework MOF-5. *Phys. Chem. Chem. Phys.* **18,** 1158–1162 (2015).
22. Bennett, T. D. & Horike, S. Liquid, glass and amorphous solid states of coordination polymers and metal–organic frameworks. *Nat. Rev. Mater.* **3,** 431–440 (2018).
23. Zhou, C. *et al.* Thermodynamic features and enthalpy relaxation in a metal–organic framework glass. *Phys. Chem. Chem. Phys.* **20,** 18291–18296 (2018).
24. Keen, D. A. & Bennett, T. D. Structural investigations of amorphous metal–organic frameworks formed via different routes. *Phys. Chem. Chem. Phys.* **20,** 7857–7861 (2018).
25. Longley, L. *et al.* Flux melting of metal–organic frameworks. *Chem. Sci.* (2019). doi:10.1039/C8SC04044C
26. Hu, Y. H. & Zhang, L. Amorphization of metal-organic framework MOF-5 at unusually low applied pressure. *Phys. Rev. B* **81,** 174103 (2010).
27. Erkartal, M. & Durandurdu, M. Pressure-Induced Amorphization of MOF-5: A First Principles Study. *ChemistrySelect* **3,** 8056–8063 (2018).
28. Bennett, T. D. *et al.* Reversible pressure-induced amorphization of a zeolitic imidazolate framework (ZIF-4). *Chem. Commun.* **47,** 7983–7985 (2011).
29. Eigen, M. Fast Elementary Steps in Chemical Reaction Mechanisms. *Pure Appl. Chem.* **6,** 97–115 (1963).

30. Férey, G. *et al.* A chromium terephthalate-based solid with unusually large pore volumes and surface area. *Science* **309,** 2040–2 (2005).
31. Millange, F., Serre, C. & Férey, G. Synthesis, structure determination and properties of MIL-53as and MIL-53ht: The first CrIII hybrid inorganic-organic microporous solids: CrIII(OH)·(O2C-C6H4-CO2)·(HO2C-C6H4-CO2H)x. *Chem. Commun.* **2,** 822–823 (2002).
32. Hamon, L. *et al.* Molecular Insight into the Adsorption of H 2 S in the Flexible MIL-53 (Cr) and Rigid MIL-47 (V) MOFs : Infrared Spectroscopy Combined to Molecular Simulations. *J. Phys. Chem. C* **115,** 2047–2056 (2011).
33. Kang, I. J., Khan, N. A., Haque, E. & Jhung, S. H. Chemical and Thermal Stability of Isotypic Metal-Organic Frameworks: Effect of Metal Ions. *Chem. - A Eur. J.* **17,** 6437–6442 (2011).
34. Rosi, N. L. *et al.* Rod packings and metal-organic frameworks constructed from rod-shaped secondary building units. *J. Am. Chem. Soc.* **127,** 1504–1518 (2005).
35. Dietzel, P. D. C., Panella, B., Hirscher, M., Blom, R. & Fjellvåg, H. Hydrogen adsorption in a nickel based coordination polymer with open metal sites in the cylindrical cavities of the desolvated framework. *Chem. Commun. (Camb).* **1,** 959–961 (2006).
36. Jiao, Y. *et al.* Tuning the Kinetic Water Stability and Adsorption Interactions of Mg-MOF-74 by Partial Substitution with Co or Ni. *Ind. Eng. Chem. Res.* **54,** 12408–12414 (2015).
37. Li, H. *et al.* Enhanced hydrostability in Ni-doped MOF-5. *Inorg. Chem.* **51,** 9200–9207 (2012).
38. Liao, P.-Q. *et al.* Drastic enhancement of catalytic activity via post-oxidation of a porous MnII triazolate framework. *Chem. - A Eur. J.* **20,** 11303–7 (2014).
39. Liao, P.-Q. *et al.* Monodentate hydroxide as a super strong yet reversible active site for CO_2 capture from high-humidity flue gas. *Energy Environ. Sci.* **8,** 1011–1016 (2015).
40. Rieth, A. J., Tulchinsky, Y. & Dincă, M. High and Reversible Ammonia Uptake in Mesoporous Azolate Metal-Organic Frameworks with Open Mn, Co, and Ni Sites. *J. Am. Chem. Soc.* **138,** 9401–9404 (2016).
41. Rieth, A. J., Yang, S., Wang, E. N. & Dincă, M. Record Atmospheric Fresh Water Capture and Heat Transfer with a Material Operating at the Water Uptake Reversibility Limit. *ACS Cent. Sci.* **3,** 668–672 (2017).
42. Rieth, A. J. & Dincă, M. Controlled Gas Uptake in Metal-Organic Frameworks with Record Ammonia Sorption. *J. Am. Chem. Soc.* **140,** 3461–3466 (2018).
43. Rieth, A. J. *et al.* Tunable Metal–Organic Frameworks Enable High-Efficiency Cascaded Adsorption Heat Pumps. *J. Am. Chem. Soc.* **140,** 17591–17596 (2018).
44. Irving, H. & Williams, R. J. P. Order of Stability of Metal Complexes. *Nature* **162,** 746–747 (1948).
45. Irving, H. & Williams, R. J. P. The stability of transition-metal complexes. *J. Chem. Soc.* 3192 (1953). doi:10.1039/jr9530003192
46. Choi, H. J., Dincă, M. & Long, J. R. Broadly Hysteretic H 2 Adsorption in the Microporous Metal−Organic Framework Co(1,4-benzenedipyrazolate). *J. Am. Chem. Soc.* **130,** 7848–7850 (2008).
47. Choi, H. J., Dincă, M., Dailly, A. & Long, J. R. Hydrogen storage in water-stable metal–organic frameworks incorporating 1,3- and 1,4-benzenedipyrazolate. *Energy Environ. Sci.* **3,** 117–123 (2010).

48. Wade, C. R., Corrales-Sanchez, T., Narayan, T. C. & Dincă, M. Postsynthetic tuning of hydrophilicity in pyrazolate MOFs to modulate water adsorption properties. *Energy Environ. Sci.* **6,** 2172 (2013).
49. Colombo, V. *et al.* High thermal and chemical stability in pyrazolate-bridged metal–organic frameworks with exposed metal sites. *Chem. Sci.* **2,** 1311 (2011).
50. Low, J. J. *et al.* Virtual High Throughput Screening Confirmed Experimentally: Porous Coordination Polymer Hydration. *J. Am. Chem. Soc.* **131,** 15834–15842 (2009).
51. Olmstead, W. N., Margolin, Z. & Bordwell, F. G. Acidities of water and simple alcohols in dimethyl sulfoxide solution. *J. Org. Chem.* **45,** 3295–3299 (1980).
52. Bordwell, F. G. Equilibrium acidities in dimethyl sulfoxide solution. *Acc. Chem. Res.* **21,** 456–463 (1988).
53. Richens, D. T. Ligand Substitution Reactions at Inorganic Centers †. *Chem. Rev.* **105,** 1961–2002 (2005).
54. Helm, L. & Merbach, A. E. Inorganic and Bioinorganic Solvent Exchange Mechanisms. *Chem. Rev.* **105,** 1923–1960 (2005).
55. Evans, D. A. Evans pKa. (2005). Available at: http://evans.rc.fas.harvard.edu/pdf/evans_pKa_table.pdf.
56. Mondloch, J. E. *et al.* Vapor-Phase Metalation by Atomic Layer Deposition in a Metal–Organic Framework. *J. Am. Chem. Soc.* **135,** 10294–10297 (2013).
57. Lillerud, K. P. *et al.* A New Zirconium Inorganic Building Brick Forming Metal Organic Frameworks with Exceptional Stability. *J. Am. Chem. Soc.* **130,** 13850–13851 (2008).
58. Furukawa, H. *et al.* Water adsorption in porous metal-organic frameworks and related materials. *J. Am. Chem. Soc.* **136,** 4369–81 (2014).
59. Li, H., Cosio, M., Wang, K., Burtner, W. & Zhou, H.-C. *Design and construction of chemically stable metal-organic frameworks*. *Elaboration and Applications of Metal-organic Frameworks* (2018). doi:10.1142/9789813226739_0001
60. Burtch, N. C., Jasuja, H. & Walton, K. S. Water Stability and Adsorption in Metal − Organic Frameworks. *Chem. Rev.* **114,** 10575–10612 (2014).
61. Nguyen, J. G. & Cohen, S. M. Moisture-Resistant and Superhydrophobic Metal−Organic Frameworks Obtained via Postsynthetic Modification. *J. Am. Chem. Soc.* **132,** 4560–4561 (2010).
62. Li, T. *et al.* Systematic modulation and enhancement of CO2 : N2 selectivity and water stability in an isoreticular series of bio-MOF-11 analogues. *Chem. Sci.* **4,** 1746–1755 (2013).
63. Makal, T. A., Wang, X. & Zhou, H.-C. Tuning the Moisture and Thermal Stability of Metal–Organic Frameworks through Incorporation of Pendant Hydrophobic Groups. *Cryst. Growth Des.* **13,** 4760–4768 (2013).
64. Jasuja, H., Huang, Y. & Walton, K. S. Adjusting the stability of metal-organic frameworks under humid conditions by ligand functionalization. *Langmuir* **28,** 16874–80 (2012).
65. Reinsch, H. *et al.* Structures, sorption characteristics, and nonlinear optical properties of a new series of highly stable aluminum MOFs. *Chem. Mater.* **25,** 17–26 (2013).
66. Huang, X. C., Lin, Y. Y., Zhang, J. P. & Chen, X. M. Ligand-directed strategy for zeolite-type metal-organic frameworks: Zinc(II) imidazolates with unusual zeolitic topologies. *Angew. Chemie - Int. Ed.* **45,** 1557–1559 (2006).
67. Masciocchi, N. *et al.* Cubic octanuclear Ni(II) clusters in highly porous polypyrazolyl-

based materials. *J. Am. Chem. Soc.* **132,** 7902–4 (2010).
68. Tan, K. *et al.* Water Reaction Mechanism in Metal Organic Frameworks with Coordinatively Unsaturated Metal Ions: MOF-74. *Chem. Mater.* **26,** 6886–6895 (2014).
69. Al-Janabi, N., Alfutimie, A., Siperstein, F. R. & Fan, X. Underlying mechanism of the hydrothermal instability of Cu3(BTC)2 metal-organic framework. *Front. Chem. Sci. Eng.* **10,** 103–107 (2016).
70. Gul-E-Noor, F. *et al.* Effects of varying water adsorption on a Cu3(BTC)2 metal-organic framework (MOF) as studied by 1H and 13C solid-state NMR spectroscopy. *Phys. Chem. Chem. Phys.* **13,** 7783–8 (2011).
71. McHugh, L. N. *et al.* Hydrolytic stability in hemilabile metal–organic frameworks. *Nat. Chem.* **10,** (2018).
72. Tian, Y. *et al.* Synthesis and structural characterization of a single-crystal to single-crystal transformable coordination polymer. *Dalt. Trans.* **43,** 1519–1523 (2014).
73. Towsif Abtab, S. M. *et al.* Reticular Chemistry in Action: A Hydrolytically Stable MOF Capturing Twice Its Weight in Adsorbed Water. *Chem* **4,** 94–105 (2018).
74. Howarth, A. J. *et al.* Chemical, thermal and mechanical stabilities of metal–organic frameworks. *Nat. Rev. Mater.* **1,** 15018 (2016).
75. Peterson, G. W. *et al.* Ammonia vapor removal by Cu 3(BTC) 2 and its characterization by MAS NMR. *J. Phys. Chem. C* **113,** 13906–13917 (2009).
76. Hungerford, J. *et al.* DMOF-1 as a Representative MOF for SO2 Adsorption in Both Humid and Dry Conditions. *J. Phys. Chem. C* **122,** 23493–23500 (2018).
77. Ruhl, A. S. & Kranzmann, A. Investigation of corrosive effects of sulphur dioxide , oxygen and water vapour on pipeline steels. *Int. J. Greenh. Gas Control* **13,** 9–16 (2013).
78. Elder, A. C., Bhattacharyya, S., Nair, S. & Orlando, T. M. Reactive Adsorption of Humid SO2 on Metal–Organic Framework Nanosheets. *J. Phys. Chem. C* **122,** 10413–10422 (2018).
79. Brozek, C. K., Miller, J. T., Stoian, S. A. & Dincă, M. NO Disproportionation at a Mononuclear Site-Isolated Fe 2+ Center in Fe 2+ -MOF-5. *J. Am. Chem. Soc.* **137,** 7495–7501 (2015).
80. McGrath, D. T. D. *et al.* Selective Decontamination of the Reactive Air Pollutant Nitrous Acid via Node-Linker Cooperativity in a Metal-Organic Framework. *Chem. Sci.* (2019). doi:10.1039/C9SC01357A
81. Carter, J. H. *et al.* Exceptional Adsorption and Binding of Sulfur Dioxide in a Robust Zirconium-Based Metal-Organic Framework. *J. Am. Chem. Soc.* **4,** 8–11 (2018).
82. Canivet, J., Fateeva, A., Guo, Y., Coasne, B. & Farrusseng, D. Water adsorption in MOFs: fundamentals and applications. *Chem. Soc. Rev.* **43,** 5594–5617 (2014).
83. Liu, J. *et al.* Stability Effects on CO2 Adsorption for the DOBDC Series of Metal–Organic Frameworks. *Langmuir* **27,** 11451–11456 (2011).
84. Campbell, M. G., Sheberla, D., Liu, S. F., Swager, T. M. & Dinc\ua, M. Cu3 (hexaiminotriphenylene) 2: an electrically conductive 2D metal--organic framework for chemiresistive sensing. *Angew. Chemie Int. Ed.* **54,** 4349–4352 (2015).
85. Park, S. S., Rieth, A. J., Hendon, C. H. & Dinca, M. Selective Vapor Pressure Dependent Proton Transport in a Metal − Organic Framework with Two Distinct Hydrophilic Pores. *J. Am. Chem. Soc.* **140,** 2016–2019 (2018).
86. Cui, S. *et al.* Metal-Organic Frameworks as advanced moisture sorbents for energy-efficient high temperature cooling. *Sci. Rep.* **8,** 15284 (2018).

87. Abdulhalim, R. G. *et al.* A Fine-Tuned Metal-Organic Framework for Autonomous Indoor Moisture Control. *J. Am. Chem. Soc.* **139,** 10715–10722 (2017).
88. Critoph, R. E. Evaluation of alternative refrigerant-adsorbent pairs for refrigeration cycles. *Appl. Therm. Eng.* **16,** 891–900 (1996).
89. De Lange, M. F., Verouden, K. J. F. M., Vlugt, T. J. H., Gascon, J. & Kapteijn, F. Adsorption-Driven Heat Pumps: The Potential of Metal-Organic Frameworks. *Chem. Rev.* **115,** 12205–12250 (2015).
90. Kalmutzki, M. J., Diercks, C. S. & Yaghi, O. M. Metal-Organic Frameworks for Water Harvesting from Air. *Adv. Mater.* **30,** 1704304 (2018).
91. Trapani, F., Polyzoidis, A., Loebbecke, S. & Piscopo, C. G. On the general water harvesting capability of metal-organic frameworks under well-defined climatic conditions. *Microporous Mesoporous Mater.* **230,** 20–24 (2016).
92. Kim, H. *et al.* Adsorption-based atmospheric water harvesting device for arid climates. *Nat. Commun.* **9,** 1191 (2018).
93. Kim, H. *et al.* Water harvesting from air with metal-organic frameworks powered by natural sunlight. *Science* **356,** 430–434 (2017).
94. Fathieh, F. *et al.* Practical water production from desert air. *Sci. Adv.* **4,** 1–10 (2018).
95. Canivet, J. *et al.* Structure–property relationships of water adsorption in metal–organic frameworks. *New J. Chem.* **38,** 3102 (2014).
96. Jeremias, F., Lozan, V., Henninger, S. K. & Janiak, C. Programming MOFs for water sorption: amino-functionalized MIL-125 and UiO-66 for heat transformation and heat storage applications. *Dalton Trans.* **42,** 15967–73 (2013).
97. Akiyama, G. *et al.* Effect of functional groups in MIL-101 on water sorption behavior. *Microporous Mesoporous Mater.* **157,** 89–93 (2012).
98. Khutia, A., Rammelberg, H. U., Schmidt, T., Henninger, S. & Janiak, C. Water Sorption Cycle Measurements on Functionalized MIL-101Cr for Heat Transformation Application. *Chem. Mater.* **25,** 790–798 (2013).
99. Wright, A. M., Rieth, A. J., Yang, S., Wang, E. & Dinca, M. Precise control of pore hydrophilicity enabled by post-synthetic cation exchange in metal-organic frameworks. *Chem. Sci.* **9,** 3856 (2018).
100. Jasuja, H., Zang, J., Sholl, D. S. & Walton, K. S. Rational tuning of water vapor and CO 2 adsorption in highly stable Zr-based MOFs. *J. Phys. Chem. C* **116,** 23526–23532 (2012).
101. Wißmann, G. *et al.* Modulated synthesis of Zr-fumarate MOF. *Microporous Mesoporous Mater.* **152,** 64–70 (2012).
102. Schaate, A. *et al.* Porous Interpenetrated Zirconium-Organic Frameworks (PIZOFs): A Chemically Versatile Family of Metal-Organic Frameworks. *Chem. - A Eur. J.* **17,** 9320–9325 (2011).
103. DeCoste, J. B., Demasky, T. J., Katz, M. J., Farha, O. K. & Hupp, J. T. A UiO-66 analogue with uncoordinated carboxylic acids for the broad-spectrum removal of toxic chemicals. *New J. Chem.* **39,** 2396–2399 (2015).
104. Wu, H. *et al.* Unusual and Highly Tunable Missing-Linker Defects in Zirconium Metal–Organic Framework UiO-66 and Their Important Effects on Gas Adsorption. *J. Am. Chem. Soc.* **135,** 10525–10532 (2013).
105. Vermoortele, F. *et al.* Synthesis Modulation as a Tool To Increase the Catalytic Activity of Metal–Organic Frameworks: The Unique Case of UiO-66(Zr). *J. Am. Chem. Soc.* **135,** 11465–11468 (2013).

106. Shearer, G. C. *et al.* Defect Engineering: Tuning the Porosity and Composition of the Metal–Organic Framework UiO-66 via Modulated Synthesis. *Chem. Mater.* **28,** 3749–3761 (2016).
107. Wang, S. *et al.* A robust large-pore zirconium carboxylate metal–organic framework for energy-efficient water-sorption-driven refrigeration. *Nat. Energy* **3,** 985–993 (2018).
108. Volkringer, C. *et al.* Synthesis, single-crystal X-ray microdiffraction, and NMR characterizations of the giant pore metal-organic framework aluminum trimesate MIL-100. *Chem. Mater.* **21,** 5695–5697 (2009).
109. Jeremias, F., Khutia, A., Henninger, S. K. & Janiak, C. MIL-100(Al, Fe) as water adsorbents for heat transformation purposes—a promising application. *J. Mater. Chem.* **22,** 10148 (2012).
110. Loiseau, T. *et al.* A Rationale for the Large Breathing of the Porous Aluminum Terephthalate (MIL-53) Upon Hydration. *Chem. - A Eur. J.* **10,** 1373–1382 (2004).
111. Kummer, H. *et al.* A Functional Full-Scale Heat Exchanger Coated with Aluminum Fumarate Metal–Organic Framework for Adsorption Heat Transformation. *Ind. Eng. Chem. Res.* **56,** 8393–8398 (2017).
112. Fröhlich, D. *et al.* Water adsorption behaviour of CAU-10-H: A thorough investigation of its structure-property relationships. *J. Mater. Chem. A* **4,** 11859–11869 (2016).
113. Fröhlich, D., Henninger, S. K. & Janiak, C. Multicycle water vapour stability of microporous breathing MOF aluminium isophthalate CAU-10-H. *Dalt. Trans.* **43,** 15300–15304 (2014).
114. Lenzen, D. *et al.* Scalable Green Synthesis and Full-Scale Test of the Metal-Organic Framework CAU-10-H for Use in Adsorption-Driven Chillers. *Adv. Mater.* **30,** 1705869 (2018).
115. Cadiau, A. *et al.* Design of Hydrophilic Metal Organic Framework Water Adsorbents for Heat Reallocation. *Adv. Mater.* **27,** 4775–4780 (2015).
116. Küsgens, P. *et al.* Characterization of metal-organic frameworks by water adsorption. *Microporous Mesoporous Mater.* **120,** 325–330 (2009).
117. Ehrenmann, J., Henninger, S. K. & Janiak, C. Water Adsorption Characteristics of MIL-101 for Heat-Transformation Applications of MOFs. *Eur. J. Inorg. Chem.* **2011,** 471–474 (2011).
118. Seo, Y.-K. *et al.* Energy-efficient dehumidification over hierachically porous metal-organic frameworks as advanced water adsorbents. *Adv. Mater.* **24,** 806–10 (2012).
119. Alezi, D. *et al.* MOF Crystal Chemistry Paving the Way to Gas Storage Needs: Aluminum-Based soc -MOF for CH4, O2, and CO2 Storage. *J. Am. Chem. Soc.* **137,** 13308–13318 (2015).
120. Chen, Z. *et al.* Reticular Access to Highly Porous acs -MOFs with Rigid Trigonal Prismatic Linkers for Water Sorption. *J. Am. Chem. Soc.* jacs.8b13710 (2019). doi:10.1021/jacs.8b13710
121. Sohail, M. *et al.* Synthesis of Highly Crystalline NH2-MIL-125 (Ti) with S-Shaped Water Isotherms for Adsorption Heat Transformation. *Cryst. Growth Des.* **17,** 1208–1213 (2017).
122. Wang, K. *et al.* Pyrazolate-Based Porphyrinic Metal–Organic Framework with Extraordinary Base-Resistance. *J. Am. Chem. Soc.* **138,** 914–919 (2016).
123. Padial, N. M. *et al.* Highly hydrophobic isoreticular porous metal-organic frameworks for the capture of harmful volatile organic compounds. *Angew. Chem. Int. Ed. Engl.* **52,**

8290–4 (2013).
124. Denysenko, D. *et al.* Elucidating gating effects for hydrogen sorption in MFU-4-type triazolate-based metal-organic frameworks featuring different pore sizes. *Chem. - A Eur. J.* **17,** 1837–1848 (2011).
125. Denysenko, D., Grzywa, M., Jelic, J., Reuter, K. & Volkmer, D. Scorpionate-type coordination in MFU-4l metal-organic frameworks: Small-molecule binding and activation upon the thermally activated formation of open metal sites. *Angew. Chemie - Int. Ed.* **53,** 5832–5836 (2014).
126. Yuhas, B. D., Mowat, J. P. S., Miller, M. A. & Sinkler, W. AlPO-78: A 24-Layer ABC-6 Aluminophosphate Synthesized Using a Simple Structure-Directing Agent. *Chem. Mater.* **30,** 582–586 (2018).
127. Shustova, N. B., Cozzolino, A. F., Reineke, S., Baldo, M. & Dincă, M. Selective Turn-On Ammonia Sensing Enabled by High-Temperature Fluorescence in Metal–Organic Frameworks with Open Metal Sites. *J. Am. Chem. Soc.* **135,** 13326–13329 (2013).
128. Campbell, M. G., Sheberla, D., Liu, S. F., Swager, T. M. & Dincă, M. Cu 3 (hexaiminotriphenylene) 2 : An Electrically Conductive 2D Metal-Organic Framework for Chemiresistive Sensing. *Angew. Chemie Int. Ed.* **54,** 4349–4352 (2015).
129. Smith, M. K., Jensen, K. E., Pivak, P. A. & Mirica, K. A. Direct Self-Assembly of Conductive Nanorods of Metal–Organic Frameworks into Chemiresistive Devices on Shrinkable Polymer Films. *Chem. Mater.* **28,** 5264–5268 (2016).
130. Bobbitt, N. S. *et al.* Metal–organic frameworks for the removal of toxic industrial chemicals and chemical warfare agents. *Chem. Soc. Rev.* **46,** 3357–3385 (2017).
131. Chen, Y., Li, L., Li, J., Ouyang, K. & Yang, J. Ammonia capture and flexible transformation of M-2(INA) (M=Cu, Co, Ni, Cd) series materials. *J. Hazard. Mater.* **306,** 340–347 (2016).
132. Barea, E., Montoro, C. & Navarro, J. A. R. Toxic gas removal – metal–organic frameworks for the capture and degradation of toxic gases and vapours. *Chem. Soc. Rev.* **43,** 5419–5430 (2014).
133. Decoste, J. B. & Peterson, G. W. Metal-organic frameworks for air purification of toxic chemicals. *Chem. Rev.* **114,** 5695–5727 (2014).
134. NIOSH. Immediately Dangerous to Life os Health Concentrations: Ammonia. (1994).
135. Woellner, M. *et al.* Adsorption and Detection of Hazardous Trace Gases by Metal–Organic Frameworks. *Adv. Mater.* **30,** 1–27 (2018).
136. Petit, C. *et al.* Toward understanding reactive adsorption of ammonia on Cu-MOF/graphite oxide nanocomposites. *Langmuir* **27,** 13043–51 (2011).
137. Kajiwara, T. *et al.* A Systematic Study on the Stability of Porous Coordination Polymers against Ammonia. *Chem. - A Eur. J.* **20,** 15611–15617 (2014).
138. DeCoste, J. B., Denny, Jr., M. S., Peterson, G. W., Mahle, J. J. & Cohen, S. M. Enhanced aging properties of HKUST-1 in hydrophobic mixed-matrix membranes for ammonia adsorption. *Chem. Sci.* **7,** 2711–2716 (2016).
139. Grant Glover, T., Peterson, G. W., Schindler, B. J., Britt, D. & Yaghi, O. MOF-74 building unit has a direct impact on toxic gas adsorption. *Chem. Eng. Sci.* **66,** 163–170 (2011).
140. Katz, M. J. *et al.* High volumetric uptake of ammonia using Cu-MOF-74/Cu-CPO-27. *Dalton Trans.* **45,** 4150–4153 (2016).
141. Britt, D., Tranchemontagne, D. & Yaghi, O. M. Metal-organic frameworks with high

capacity and selectivity for harmful gases. *Proc. Natl. Acad. Sci. U. S. A.* **105,** 11623–11627 (2008).
142. Petit, C. & Bandosz, T. J. Enhanced Adsorption of Ammonia on Metal-Organic Framework/Graphite Oxide Composites: Analysis of Surface Interactions. *Adv. Funct. Mater.* **20,** 111–118 (2010).
143. Spanopoulos, I., Xydias, P., Malliakas, C. D. & Trikalitis, P. N. A Straight Forward Route for the Development of Metal–Organic Frameworks Functionalized with Aromatic −OH Groups: Synthesis, Characterization, and Gas (N 2 , Ar, H 2 , CO 2 , CH 4 , NH 3) Sorption Properties. *Inorg. Chem.* **52,** 855–862 (2013).
144. Jasuja, H., Peterson, G. W., Decoste, J. B., Browe, M. A. & Walton, K. S. Evaluation of MOFs for air purification and air quality control applications: Ammonia removal from air. *Chem. Eng. Sci.* **124,** 118–124 (2015).
145. Joshi, J. N., Garcia-Gutierrez, E. Y., Moran, C. M., Deneff, J. I. & Walton, K. S. Engineering Copper Carboxylate Functionalities on Water Stable Metal-Organic Frameworks for Enhancement of Ammonia Removal Capacities. *J. Phys. Chem. C* **121,** 3310–3319 (2017).
146. Morris, W., Doonan, C. J. & Yaghi, O. M. Postsynthetic modification of a metal-organic framework for stabilization of a hemiaminal and ammonia uptake. *Inorg. Chem.* **50,** 6853–6855 (2011).
147. Godfrey, H. G. W. *et al.* Ammonia Storage by Reversible Host-Guest Site Exchange in a Robust Metal-Organic Framework. *Angew. Chemie Int. Ed.* **57,** 14778–14781 (2018).
148. Wilcox, O. T. *et al.* Acid loaded porphyrin-based metal-organic framework for ammonia uptake. *Chem. Commun.* **51,** 14989–14991 (2015).
149. Van Humbeck, J. F. *et al.* Ammonia capture in porous organic polymers densely functionalized with Brønsted acid groups. *J. Am. Chem. Soc.* **136,** 2432–40 (2014).
150. Takahashi, A. *et al.* Historical Pigment Exhibiting Ammonia Gas Capture beyond Standard Adsorbents with Adsorption Sites of Two Kinds. *J. Am. Chem. Soc.* **138,** 6376–6379 (2016).
151. Doonan, C. J., Tranchemontagne, D. J., Glover, T. G., Hunt, J. R. & Yaghi, O. M. Exceptional ammonia uptake by a covalent organic framework. *Nat. Chem.* **2,** 235–8 (2010).
152. Barin, G. *et al.* Highly effective ammonia removal in a series of Brønsted acidic porous polymers: investigation of chemical and structural variations. *Chem. Sci.* **8,** 4399–4409 (2017).
153. Huberty, M. S., Wagner, A. L., McCormick, A. & Cussler, E. Ammonia absorption at haber process conditions. *AIChE J.* **58,** 3526–3532 (2012).
154. Petit, C., Mendoza, B. & Bandosz, T. J. Reactive adsorption of ammonia on Cu-based MOF/graphene composites. *Langmuir* **26,** 15302–15309 (2010).
155. OSHA. Safety and Health Topics: Hydrogen Sulfide.
156. Vikrant, K., Kumar, V., Ok, Y. S., Kim, K.-H. & Deep, A. Metal-organic framework (MOF)-based advanced sensing platforms for the detection of hydrogen sulfide. *TrAC Trends Anal. Chem.* **105,** 263–281 (2018).
157. Yassine, O. *et al.* H 2 S Sensors: Fumarate-Based fcu-MOF Thin Film Grown on a Capacitive Interdigitated Electrode. *Angew. Chemie Int. Ed.* **55,** 15879–15883 (2016).
158. Wan, X., Wu, L., Zhang, L., Song, H. & Lv, Y. Sensors and Actuators B : Chemical Novel metal-organic frameworks-based hydrogen sulfide cataluminescence sensors. **220,** 614–

621 (2015).
159. Petit, C., Levasseur, B., Mendoza, B. & Bandosz, T. J. Reactive adsorption of acidic gases on MOF/graphite oxide composites. *Microporous Mesoporous Mater.* **154,** 107–112 (2012).
160. Petit, C., Mendoza, B. & Bandosz, T. J. Hydrogen Sulfide Adsorption on MOFs and MOF/Graphite Oxide Composites. *ChemPhysChem* **11,** 3678–3684 (2010).
161. Nickerl, G. *et al.* Integration of accessible secondary metal sites into MOFs for H2S removal. *Inorg. Chem. Front.* **1,** 325–330 (2014).
162. Joshi, J. N. *et al.* Probing Metal-Organic Framework Design for Adsorptive Natural Gas Purification. *Langmuir* **34,** 8443–8450 (2018).
163. Sánchez-González, E. *et al.* Highly reversible sorption of H 2 S and CO 2 by an environmentally friendly Mg-based MOF. *J. Mater. Chem. A* **6,** 16900–16909 (2018).
164. Belmabkhout, Y. *et al.* Natural gas upgrading using a fluorinated MOF with tuned H2S and CO2 adsorption selectivity. *Nat. Energy* **3,** 1059–1066 (2018).
165. Cadiau, A., Adil, K., Bhatt, P. M., Belmabkhout, Y. & Eddaoudi, M. A metal-organic framework-based splitter for separating propylene from propane. *Science* **353,** 137–140 (2016).
166. Liu, G. *et al.* Enabling Fluorinated MOF-Based Membranes for Simultaneous Removal of H 2 S and CO 2 from Natural Gas. *Angew. Chemie Int. Ed.* **57,** 14811–14816 (2018).
167. Subramanian, S. & Zaworotko, M. J. Porous Solids by Design:[Zn(4,4′-bpy)2(SiF6)]n·xDMF, a Single Framework Octahedral Coordination Polymer with Large Square Channels. *Angew. Chemie Int. Ed. English* **34,** 2127–2129 (1995).
168. Cadiau, A. *et al.* Molecular sorption: Hydrolytically stable fluorinated metal-organic frameworks for energy-efficient dehydration. *Science* **356,** 731–735 (2017).
169. Mohideen, M. I. H. *et al.* A Fine-Tuned MOF for Gas and Vapor Separation: A Multipurpose Adsorbent for Acid Gas Removal, Dehydration, and BTX Sieving. *Chem* **3,** 822–833 (2017).
170. EPA. National Trends in Sulfur Dioxide Emissions. Available at: https://www.epa.gov/air-trends/sulfur-dioxide-trends.
171. Córdoba, P. Status of Flue Gas Desulphurisation (FGD) systems from coal-fired power plants: Overview of the physic-chemical control processes of wet limestone FGDs. *Fuel* **144,** 274–286 (2015).
172. EPA. Coal Fired Power Plant Data. Available at: https://www.epa.gov/airmarkets/coal-fired-power-plant-data.
173. Ding, L. & Yazaydin, A. O. The effect of SO2 on CO2 capture in zeolitic imidazolate frameworks. *Phys. Chem. Chem. Phys.* **15,** 11856 (2013).
174. Pacciani, R. *et al.* Influence of the concentration of CO 2 and SO 2 on the absorption of CO 2 by a lithium orthosilicate-based absorbent. *Environ. Sci. Tech.* **45,** 7083–7088 (2011).
175. Han, X., Yang, S. & Schröder, M. Porous metal–organic frameworks as emerging sorbents for clean air. *Nat. Rev. Chem.* **3,** 108–118 (2019).
176. Mounfield, W. P. *et al.* Synergistic Effects of Water and SO2 on Degradation of MIL-125 in the Presence of Acid Gases. *J. Phys. Chem. C* **120,** 27230–27240 (2016).
177. Yang, S. *et al.* Irreversible Network Transformation in a Dynamic Porous Host Catalyzed by Sulfur Dioxide. *J. Am. Chem. Soc.* **135,** 4954–4957 (2013).
178. Yang, S. *et al.* Selectivity and direct visualization of carbon dioxide and sulfur dioxide in

a decorated porous host. *Nat. Chem.* **4,** 887–894 (2012).
179. Li, L. *et al.* Post-synthetic modulation of the charge distribution in a metal–organic framework for optimal binding of carbon dioxide and sulfur dioxide. *Chem. Sci.* **10,** 1472–1482 (2019).
180. Britt, D., Tranchemontagne, D. & Yaghi, O. M. Metal-organic frameworks with high capacity and selectivity for harmful gases. *Proc. Nat. Acad. Sci.* **105,** 11623–11627 (2008).
181. Tan, K. *et al.* Mechanism of Preferential Adsorption of SO 2 into Two Microporous Paddle Wheel Frameworks M(bdc)(ted) 0.5. *Chem. Mater.* **25,** 4653–4662 (2013).
182. Cui, X. *et al.* Ultrahigh and Selective SO2 Uptake in Inorganic Anion-Pillared Hybrid Porous Materials. *Adv. Mater.* **29,** 1–9 (2017).
183. Tchalala, M. R. *et al.* Fluorinated MOF platform for selective removal and sensing of SO2 from flue gas and air. *Nat. Commun.* **10,** 1328 (2019).
184. Rodríguez-Albelo, L. M. *et al.* Selective sulfur dioxide adsorption on crystal defect sites on an isoreticular metal organic framework series. *Nat. Commun.* **8,** (2017).
185. Bhattacharyya, S. *et al.* Interactions of SO2 -Containing Acid Gases with ZIF-8: Structural Changes and Mechanistic Investigations. *J. Phys. Chem. C* **120,** 27221–27229 (2016).
186. Carter, J. H. *et al.* Exceptional Adsorption and Binding of Sulfur Dioxide in a Robust Zirconium-Based Metal–Organic Framework. *J. Am. Chem. Soc.* **140,** 15564–15567 (2018).
187. Savage, M. *et al.* Selective Adsorption of Sulfur Dioxide in a Robust Metal-Organic Framework Material. *Adv. Mater.* **28,** 8705–8711 (2016).
188. Fernandez, C. A. *et al.* Gas-Induced Expansion and Contraction of a Fluorinated Metal−Organic Framework. *Cryst. Growth Des.* **10,** 1037–1039 (2010).
189. Mon, M. *et al.* A post-synthetic approach triggers selective and reversible sulphur dioxide adsorption on a metal-organic framework. *Chem. Commun.* **54,** 9063–9066 (2018).
190. Wang, C. *et al.* Agriculture is a major source of NOx pollution in California. *Sci. Adv.* **4,** 3477 (2018).
191. Crutzen, P. J. The role of NO and NO2 in the chemistry of the troposphere and stratosphere. *Ann. Rev. Earth Planet. Sci.* **7,** 443–472 (1979).
192. Wang, P. *et al.* Porous metal–organic framework MIL-100(Fe) as an efficient catalyst for the selective catalytic reduction of NO x with NH 3. *RSC Adv.* **4,** 48912–48919 (2014).
193. Jiang, H. *et al.* Effect of Cosolvent and Temperature on the Structures and Properties of Cu-MOF-74 in Low-temperature NH 3 -SCR. *Ind. Eng. Chem. Res.* **56,** 3542–3550 (2017).
194. Zhang, M., Wang, W. & Chen, Y. Theoretical investigation of selective catalytic reduction of NO on MIL-100-Fe. *Phys. Chem. Chem. Phys.* **20,** 2211–2219 (2018).
195. Granger, P. & Parvulescu, V. I. Catalytic NOxabatement systems for mobile sources: From three-way to lean burn after-treatment technologies. *Chem. Rev.* **111,** 3155–3207 (2011).
196. Bartok, W. & Sarofim, A. F. *Fossil Fuel Combustion. A Source Book.* (Wiley-Interscience, 1991).
197. *Radicals for Life. The Various Forms of Nitric Oxide*. (Elservier, 2007).
198. Keefer, L. K. Thwarting thrombus. *Nat. Mater.* **2,** 357–358 (2003).
199. Baudron, S. A. Dipyrrin based homo- and hetero-metallic infinite architectures.

CrystEngComm **12,** 2288–2295 (2010).
200. Xiao, B. *et al.* High-Capacity Hydrogen and Nitric Oxide Adsorption and Storage in a Metal−Organic Framework. *J. Am. Chem. Soc.* **129,** 1203–1209 (2007).
201. Wright, A. M., Wu, G. & Hayton, T. W. Structural Characterization of a Copper Nitrosyl Complex with a {CuNO} 10 Configuration. *J. Am. Chem. Soc.* **132,** 14336–14337 (2010).
202. Bordiga, S. *et al.* Interaction of N2, CO and NO with Cu-exchanged ETS-10: a compared FTIR study with other Cu-zeolites and with dispersed Cu2O. *Catal. Today* **70,** 91–105 (2001).
203. Peikert, K. *et al.* Tuning the nitric oxide release behavior of amino functionalized HKUST-1. *Microporous Mesoporous Mater.* **216,** 118–126 (2015).
204. McKinlay, A. C. *et al.* Nitric Oxide Adsorption and Delivery in Flexible MIL-88(Fe) Metal–Organic Frameworks. *Chem. Mater.* **25,** 1592–1599 (2013).
205. Bonino, F. *et al.* Local Structure of CPO-27-Ni Metallorganic Framework upon Dehydration and Coordination of NO. *Chem. Mater.* **20,** 4957–4968 (2008).
206. C. McKinlay, A. *et al.* Exceptional behavior over the whole adsorption-storage-delivery cycle for NO in porous metal organic frameworks. *J. Am. Chem. Soc.* **130,** 10440–10444 (2008).
207. Cattaneo, D. *et al.* Tuning the nitric oxide release from CPO-27 MOFs. *RSC Adv.* **6,** 14059–14067 (2016).
208. Bloch, E. D. *et al.* Gradual Release of Strongly Bound Nitric Oxide from Fe2(NO)2(dobdc). *J. Am. Chem. Soc.* **137,** 3466–3469 (2015).
209. Ebrahim, A. M., Levasseur, B. & Bandosz, T. J. Interactions of NO2 with Zr-Based MOF: Effects of the Size of Organic Linkers on NO2 Adsorption at Ambient Conditions. *Langmuir* **29,** 168–174 (2013).
210. Peterson, G. W., Mahle, J. J., Decoste, J. B., Gordon, W. O. & Rossin, J. A. Extraordinary NO2 removal by the metal-organic framework UiO-66-NH2. *Angew. Chem. Int. Ed.* **55,** 6235–6238 (2016).
211. Han, X. *et al.* Reversible adsorption of nitrogen dioxide within a robust porous metal–organic framework. *Nat. Mater.* **17,** 691–696 (2018).
212. Schulz, M. *et al.* A Calixarene-Based Metal–Organic Framework for Highly Selective NO2 Detection. *Angew. Chem. Int. Ed.* **57,** 12961–12965 (2018).
213. Sava, D. F. *et al.* Capture of Volatile Iodine, a Gaseous Fission Product, by Zeolitic Imidazolate Framework-8. *J. Am. Chem. Soc.* **133,** 12398–12401 (2011).
214. Sava, D. F. *et al.* Competitive I 2 Sorption by Cu-BTC from Humid Gas Streams. *Chem. Mater.* **25,** 2591–2596 (2013).
215. Falaise, C. *et al.* Capture of iodine in highly stable metal–organic frameworks: a systematic study. *Chem. Commun.* **49,** 10320 (2013).
216. Yao, R.-X., Cui, X., Jia, X.-X., Zhang, F.-Q. & Zhang, X.-M. A Luminescent Zinc(II) Metal–Organic Framework (MOF) with Conjugated π-Electron Ligand for High Iodine Capture and Nitro-Explosive Detection. *Inorg. Chem.* **55,** 9270–9275 (2016).
217. Li, B. *et al.* Capture of organic iodides from nuclear waste by metal-organic framework-based molecular traps. *Nat. Commun.* **8,** 485 (2017).
218. Zhang, X. *et al.* Confinement of Iodine Molecules into Triple-Helical Chains within Robust Metal–Organic Frameworks. *J. Am. Chem. Soc.* **139,** 16289–16296 (2017).
219. Lobanov, S. S. *et al.* Iodine in Metal–Organic Frameworks at High Pressure. *J. Phys. Chem. A* **122,** 6109–6117 (2018).

220. Banerjee, D. *et al.* Iodine Adsorption in Metal Organic Frameworks in the Presence of Humidity. *ACS App. Mater. Inter.* **10,** 10622–10626 (2018).
221. DeCoste, J. B., Browe, M. A., Wagner, G. W., Rossin, J. A. & Peterson, G. W. Removal of chlorine gas by an amine functionalized metal–organic framework via electrophilic aromatic substitution. *Chem. Commun.* **51,** 12474–12477 (2015).
222. Tulchinsky, Y. *et al.* Reversible Capture and Release of Cl2 and Br2 with a Redox-Active Metal–Organic Framework. *J. Am. Chem. Soc.* **139,** 5992–5997 (2017).
223. Brozek, C. K. & Dincă, M. Lattice-imposed geometry in metal–organic frameworks: lacunary Zn4O clusters in MOF-5 serve as tripodal chelating ligands for Ni2+. *Chem. Sci.* **3,** 2110 (2012).
224. Brozek, C. K. & Dinca, M. Cation exchange at the secondary building units of metal-organic frameworks. *Chem Soc Rev* **43,** 5456–5467 (2014).
225. Leus, K. *et al.* Systematic study of the chemical and hydrothermal stability of selected 'stable' Metal Organic Frameworks. *Microporous Mesoporous Mater.* **226,** 110–116 (2016).